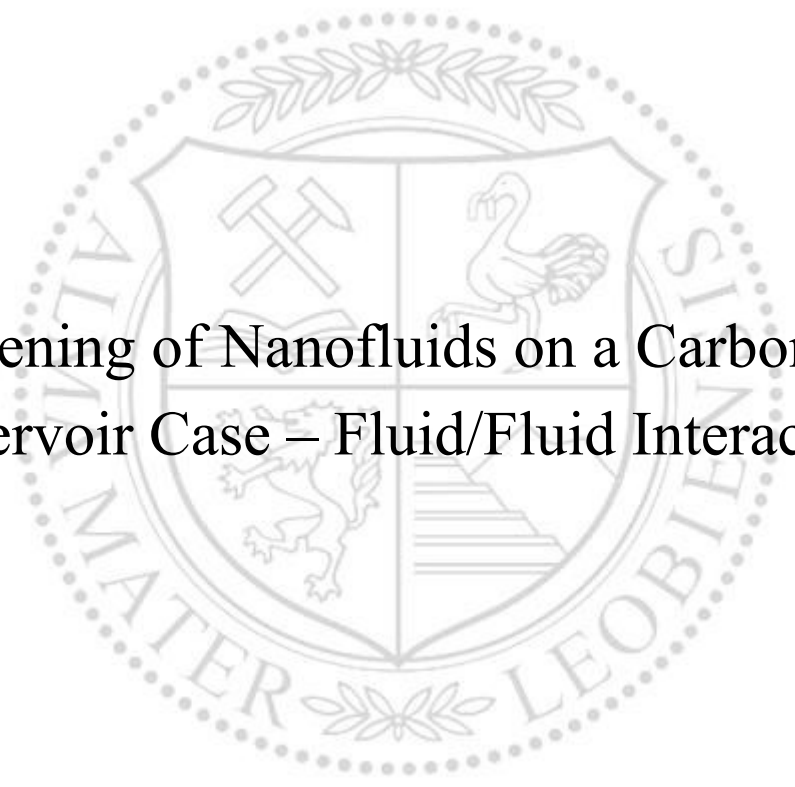




Chair of Reservoir Engineering

Master's Thesis



Screening of Nanofluids on a Carbonate  
Reservoir Case – Fluid/Fluid Interaction

Manad Almabroek Ahmed Almuzoughi

May 2021





**MONTANUNIVERSITÄT LEOBEN**  
www.unileoben.ac.at

**AFFIDAVIT**

I declare on oath that I wrote this thesis independently, did not use other than the specified sources and aids, and did not otherwise use any unauthorized aids.

I declare that I have read, understood, and complied with the guidelines of the senate of the Montanuniversität Leoben for "Good Scientific Practice".

Furthermore, I declare that the electronic and printed version of the submitted thesis are identical, both, formally and with regard to content.

Date 05.05.2021

Signature Author

Manad Almabroek Ahmed Almuzoughi

Manad Almuzoughi

Master Thesis 2020

Supervisor: Univ.-Prof. Dr. Holger Ott

Co-supervisor: Dipl.-Ing. Pit Arnold

# Screening of Nanofluids on a Carbonate Reservoir Case – Fluid/Fluid Interaction

*I do want to devote my study to my mother Ms. Raja Hashem, my father Mr. Almabrouk Almuzoughi, and all my brothers Mourad, Mouyed, Mouad, and Majed which they have all been a great help and support me during my studies period.*

## Acknowledgments

I would like to thank the chair of Reservoir Engineering at the Montan University of Leoben, especially Professor Ott Holger and Pit Arnold for providing the opportunity, information, coaching, and support needed to complete this thesis.

I would also like to thank Mr. Giuma Shita and OMV company for giving me a lot of additional support. I appreciate everyone's effort.

Finally, I want to thank my family, mentors, and close friends for supporting me during my studies. Many thanks to my parents and my brother Dr. Mourad Almuzoughi for supporting me in both moral and financial.

Special thanks to my uncle Dr. Hassan Hashem who always supported me in all my endeavors and who believed in me. Also, I want to thank my friend Zakaria Barghti for being there for me when I needed him for support.

## Abstract

This work aims to examine alkali solutions' performance and different types of nanofluids in terms of fluid-fluid interaction based on carbonate reservoir data that the OMV company provided. The interactions of low total acid number (TAN) crude oil, the composition of nanofluids, and alkali solution were studied using compatibility tests, phase behavior evaluation, and interfacial tension (IFT) measurements. At first, the compatibility screening (salinity scan) test was used to examine the influence of different alkali and nanofluids. Then, the phase behavior experiments were performed at a 1:1 oil-water ratio using low TAN crude oil. In total, almost 36 different combinations with triplicates were tested. Finally, IFT experiments were performed using a spinning-drop tensiometer, and the results were compared at approximately 150 minutes of observation.

Sodium carbonate ( $\text{Na}_2\text{CO}_3$ ) was used as the alkaline agent. Six types of nanomaterial were also used. The first three types of nanofluids have the names S1, E100, and P100, and contain silicon dioxide nanoparticles with different surface modifications. In contrast, one other had the name R1, which contains combination solvent, surfactants, and surface-modified silicon dioxide nanoparticles. The last two types of nanofluids were named A1 and A2, and they consist of silicon dioxide and aluminum oxide nanoparticles with different surface modifications.

Moreover, two synthetic brines were prepared. The first brine is rich in divalent cations such as  $\text{Ca}^{+2}$  and  $\text{Mg}^{+2}$  and was named real brine. While the second brine was called softened brine, and it contains a deficient concentration of divalent cations.

Precipitations were observed during the compatibility tests in most cases when using solutions containing nanomaterials and alkali fluids using the real brine. IFT measurements have shown that nanomaterials are significantly efficient in reducing IFT, despite the low TAN oil. However, nanofluids containing surfactants showed the best performance in generating IFT reduction, which has the lowest IFT value (0.17mN/m) compared to other nanofluids. Finally, a high emulsion volume was observed directly after mixing the samples for the phase behavior evaluations. Besides that, nanofluids alone were unable to generate considerable emulsion volumes.

Keywords: Nanofluids, IFT Reduction, Compatibility test, Phase behavior, Nanoparticle Stability



## Zusammenfassung

Diese Arbeit zielt darauf ab, die Leistung von Alkalilösungen und verschiedene Arten von Nanofluiden im Hinblick auf die Fluid-Fluid-Wechselwirkung auf der Grundlage der von der OMV-Firma bereitgestellten Karbonat-Reservoir-Daten zu untersuchen. Die Wechselwirkungen von Rohöl mit niedriger Gesamtsäurezahl (TAN), die Zusammensetzung von Nanofluiden und Alkalilösung wurden unter Verwendung von Verträglichkeitstests, Bewertung des Phasenverhaltens und Messungen der Grenzflächenspannung (IFT) untersucht. Zunächst wurde der Kompatibilitäts-Screening-Test (Salinity Scan) verwendet, um den Einfluss verschiedener Alkali- und Nanofluiden zu untersuchen. Dann wurden die Phasenverhaltensexperimente bei einem Öl-Wasser-Verhältnis von 1:1 unter Verwendung von Rohöl mit niedriger TAN durchgeführt. Insgesamt wurden fast 36 verschiedene Kombinationen mit Dreifachversuchen getestet. Schließlich wurden IFT-Experimente unter Verwendung eines Spinning-Drop-Tensiometers durchgeführt, und die Ergebnisse wurden nach ungefähr 150 Minuten Beobachtung verglichen.

Natriumcarbonat ( $\text{Na}_2\text{CO}_3$ ) wurde als alkalisches Mittel verwendet. Sechs Arten von Nanomaterialien wurden ebenfalls verwendet. Die ersten drei Arten von Nanofluiden haben die Namen S1, E100 und P100 und enthalten Siliziumdioxid-Nanopartikel mit unterschiedlichen Oberflächenmodifikationen. Im Gegensatz dazu hatte eine andere den Namen R1, der Kombinationslösungsmittel, Tenside und oberflächenmodifizierte Siliziumdioxid-Nanopartikel enthält. Die letzten beiden Arten von Nanofluiden wurden als A1 und A2 bezeichnet und bestehen aus Siliziumdioxid- und Aluminiumoxid-Nanopartikeln mit unterschiedlichen Oberflächenmodifikationen.

Darüber hinaus wurden zwei synthetische Salzlösungen hergestellt. Die erste Salzlösung ist reich an zweiwertigen Kationen wie  $\text{Ca}^{+2}$  und  $\text{Mg}^{+2}$  und wurde als echte Salzlösung bezeichnet. Während die zweite Salzlösung als erweichte Salzlösung bezeichnet wurde, enthält sie eine unzureichende Konzentration an zweiwertigen Kationen.

Während der Verträglichkeitstests wurden in den meisten Fällen Ausfällungen beobachtet, wenn Lösungen verwendet wurden, die Nanomaterialien und Alkaliflüssigkeiten enthielten, wobei die echte Salzlösung verwendet wurde. IFT-Messungen haben gezeigt, dass Nanomaterialien trotz des niedrigen TAN-Öls die IFT signifikant effizient reduzieren können.

Nanofluide, die Tenside enthalten, zeigten jedoch die beste Leistung bei der Erzeugung einer IFT-Reduktion, die im Vergleich zu anderen Nanofluiden den niedrigsten IFT-Wert (0,17mN/m) aufweist. Schließlich wurde ein hohes Emulsionsvolumen direkt nach dem Mischen der Proben für die Phasenverhaltensbewertungen beobachtet. Außerdem konnten Nanofluide allein kein nennenswertes Emulsionsvolumen erzeugen.

Schlüsselwörter: Nanofluide, IFT-Reduktion, Verträglichkeitstest, Phasenverhalten, Nanopartikelstabilität

## Table of Contents

Acknowledgments.....	vi
Abstract.....	vii
Zusammenfassung.....	ix
Chapter 1.....	1
Introduction.....	1
1.1 Background.....	1
1.2 Scope and Overview .....	2
Chapter 2.....	3
Fundamentals.....	3
2.1 Enhanced Oil Recovery Principles .....	3
2.2 Alkaline Flooding .....	4
2.3 Phase Behavior.....	6
2.4 Interfacial Tension, IFT .....	8
Chapter 3.....	11
State of the Art.....	11
3.1 Nanotechnology .....	11
3.2 Stability of Nanofluid .....	12
3.3 Influence of NPs on IFT .....	14
3.4 Effect of Nanoparticles on Stabilized Oil/Water Emulsion .....	17
Chapter 4.....	19
Experimental Setup and Materials .....	19
4.1 Fluid Preparation and Characterization.....	19
4.2 Compatibility Test .....	23
4.3 Phase Behavior Experiments .....	25
4.4 Density and Viscosity Evaluation.....	27
4.5 IFT Measurement.....	27
Chapter 5.....	31
Results and Discussion .....	31
5.1 Fluid Characterization Results.....	31
5.2 Compatibility Test .....	32
5.3 Phase Screening Evaluations .....	42
5.4 Interfacial Tension .....	56
Chapter 6.....	63
Conclusion .....	63
6.1 Future Work.....	64
Chapter 7.....	65
References.....	65

Lab Experiments Results .....A-1

## List of Figures

Figure 2-1: Schematic of the alkaline recovery process (deZabala et al., 1982). .....	5
Figure 2-2: Schematic of the surfactant molecule (Chuo et al., 2014). .....	6
Figure 2-3: Three Types of Microemulsion and the Effect of Salinity on Phase Behavior (Healy et al., 1975) .....	7
Figure 2-4 Pickering emulsion (Mcmullen & Ingredients, 2014). .....	8
Figure 2-5 Spinning drop method (Viades-Trejo & Gracia-Fadrique, 2007) .....	9
Figure 2-6: Shape of spinning drop related to interfacial tension (Arekhov, 2019) .....	10
Figure 3-1 The schematic of nanofluids mechanisms (Sun et al., 2017). .....	12
Figure 3-2 stable and unstable suspension (Mohamed et al., 2018). .....	13
Figure 3-3 IFT measurements at 60°C and 7000 rpm (a) between low TAN crude oil and brine (b) IFT measurements between high TAN crude oil and brine (Neubauer et al., 2020 a).....	15
Figure 3-4: IFT measurements between crude oil and brine/nanofluids (Neubauer et al., 2020 b) .....	16
Figure 3-5 interfacial tension W/O versus silica with different size of NPS (Jalil & Hussein, 2019).....	17
Figure 4-1 The steps process to prepare syntactic brine .....	21
Figure 4-2 Eppendorf and pipettes.....	24
Figure 4-3 Alkaline solution (softened brine) at different concentrations .....	24
Figure 4-4 Nanofluid (S1) at different concentrations for real and softened .....	24
Figure 4-5 Nanofluid (P100 & E100) for real and softened .....	25
Figure 4-6 Nanofluid (A1 & A2) at different concentration for real and softened .....	25
Figure 4-7 The workflow of a phase behavior experiment.....	26
Figure 4-8 The SVM 3000 Stainer Viscometer (Armgate, 2015).....	27
Figure 4-9 A KRUSS spinning drop tensiometer (Krüss scientific, 2018).....	28
Figure 4-10 IFT-measuring device components (Arekhov 2019).....	29
Figure 5-1 Nanofluid S1 at 10 wt%, 15wt%, 20 wt%, 25 wt%, 30 wt% (Left Real) (Right Softened) at (time 0) .....	32
Figure 5-2 Nanofluid S1 at 10 wt%, 15wt% ,20 wt%, 25 wt% , 30 wt% (Left Real) (Right Softened) (after 24 hr).....	33
Figure 5-3 Nanofluid R1 at 1 & 2 gpt (Left Real) (Right Softened) at (time 0).....	34
Figure 5-4 Nanofluid R1 at 1 & 2 gpt (Left Real) (Right Softened) (after 24 hrs.).....	35
Figure 5-5 Nanofluid P100& E100 at 0.1 wt% (Left Real) (Right Softened) at (time 0).....	36
Figure 5-6 Nanofluid P100& E100 Real at 0.1 wt% (Left Real) (Right Softened) (after 24 hrs.) .....	36
Figure 5-7 Nanofluids A1 & A2 at 10 wt% (Left Real) (Right Softened) at (time 0) .....	38
Figure 5-8 Nanofluids A1 & A2 at 20 wt% (Left Real) (Right Softened) at (time 0) .....	38
Figure 5-9 Nanofluids A1 & A2 (Left Real) (Right Softened) at 10 wt% (after 24 hrs.) .....	38
Figure 5-10 Nanofluids A1 & A2 (Left Real) (Right Softened) at 20 wt% (after 24 hrs.) .....	39
Figure 5-11 Alkaline solution (Real brine) at 10 & 20 g/l.....	40
Figure 5-12 Alkaline (NaCO <sub>3</sub> ) Softened brine at (1000-10000 ppm) at (time 0). .....	40
Figure 5-13 All nanofluids for real brine after one week of observation.....	41
Figure 5-14 All nanofluids for softened brine after one week of observation .....	41
Figure 5-15 Phase experiments (after mixing) with 10, 15, 20, 25 & 30 wt% of (S1). .....	43
Figure 5-16 Emulsion volume over 30 days and 73 °C with crude oil and nanofluid S1 Real at different concentrations. ....	43
Figure 5-17 Phase experiments with 1 & 2 gpt of nanofluid R1 .....	45
Figure 5-18 Phase experiments with nanofluids A1 & A2 at 10 wt%,.....	46
Figure 5-19 Phase experiments with nanofluid A1 & A2 at 20 wt%,.....	46
Figure 5-20 Emulsion volume over 30 days and 73 °C for nanofluid A1 Real & Softened at 10 & 20 wt% .....	48

Figure 5-21 Emulsion volume over 30 days and 73°C for nanofluid A2 Real & Softened at 10 & 20 wt% .....	48
Figure 5-22 Phase experiments with 0.1 wt% of P100 & E100.....	49
Figure 5-23 Phase experiments with 10, 15, 20, 25 & 30 wt% of (S1) Softened .....	50
Figure 5-24 Emulsion volume over 30 days and 73°C for (S1) Softened at different concentrations .....	51
Figure 5-25 Phase experiments with 1 & 2 gpt of nanofluid (R1).....	52
Figure 5-26 Phase experiments with Nanofluid A1 & A2 10 wt%.....	53
Figure 5-27 Phase experiments with nanofluid A1 & A2 20 wt% .....	54
Figure 5-28 Phase experiments with 0.1 wt% of nanofluid P100& E100, Blue lines: oil/brine interface .....	55
Figure 5-29 Phase experiments with Alkaline solution at (1000-10000) with 1000 step, Blue lines: oil/brine interface. ....	56
Figure 5-30 The IFT of real and softened brine.....	57
Figure 5-31 The IFT between nanofluid S1 (10 – 30 wt%) & nanofluid R1 and crude oil. ....	58
Figure 5-32 The IFT between nanofluid E100 & A1 and crude oil.....	58

## List of Tables

Table 4-1 Synthetic formation brine .....	20
Table 4-2 Soften brine composition.....	20
Table 4-3 Properties of crude oil samples.....	21
<i>Table 4-4: Physical and chemical properties of the nanomaterial stock solutions.</i> .....	22
Table 4-5 The values of concentrations for Nanofluids.....	26
Table 5-1 Crude oil properties .....	31
Table 5-2 Synthetic brine properties.....	31
Table 5-3 The observation of compatibility nanofluid S1 .....	34
Table 5-4 The observation of compatibility nanofluid R1 .....	35
Table 5-5 The observation of compatibility nanofluids E100 & P100 .....	37
Table 5-6 The observation of compatibility nanofluids A1 &A2 .....	39
Table 5-7 The observation of compatibility alkali solution.....	41
Table 5-8 The summary of nanofluids for real and softened brine.....	42
Table 5-9 The summary results of IFT at 73 °C and 7000 rpm between low TAN crude oil and nanofluids.....	61
Table 7-1 Na <sub>2</sub> CO <sub>3</sub> properties .....	A-1
Table 7-2 Nano clear A1 & A2.....	A-2
Table 7-3: Nanofluids E100 & P100.....	A-2
Table 7-4: Nanofluid R1 at 1 & 2 gpt for real and softened .....	A-3
Table 7-5: Nanofluid (S1) at different concentrations for real & softened.....	A-3





## Nomenclature

$r$	radius	[m]
$t$	time	[s]
$T$	Temperature	[°C]
$\mu$	viscosity	[cP]



## Abbreviations

EOR	Enhanced Oil Recovery
TAN	Total Acid Number
AN	Acid Number
IFT	Interfacial Tension
Pa	Pascal
s	second
m	meters
N	Newton
D	Darcy
g	gram
NPs	nanoparticles
O	oil phase
W	water phase
SEM	Scanning Electron Microscope
ml	milliliters
rpm	revolution per minute
Eq.	Equation
St. Dev.	Standard Deviation
St. U.	Saint Ulrich (oil)
Ft	foot
CMC	Critical micelle concentration
Nca	Capillary number
$\theta$	Contact angle
$\sigma$	IFT
v	Velocity
NaCl	Sodium chloride
Na <sub>2</sub> CO <sub>3</sub>	Sodium carbonate
Ppm	parts per million
°C	Celsius



# Chapter 1

## Introduction

### 1.1 Background

Worldwide energy demand is estimated to increase up to 50% by the end of 2030. The role of renewable resources such as wind and solar energy seems negligible in meeting this energy demand rise. Consequently, oil and gas will remain in the next few decades the dominant source of energy. The discovery of new fields and the increase in production from existing oil fields is crucial due to this expected increase in the energy demand (Kamal et al., 2017). However, enhanced oil recovery (EOR) is also crucial since any increase in the oil recovery can help to cover the expected global rise in energy demand (Cheraghian & Hendraningrat, 2016). EOR can be achieved by means of chemical, thermal, or solvent injecting. Chemical EOR is done by injecting chemicals such as surfactants, polymers, and alkali to maximize the ultimate oil and gas recovery. The alkaline injection is achieved by inciting alkaline components that have the ability to react with the acid component of oil, which may result in generating in-situ surfactants that could cause a reduction in the interfacial tension (IFT) and an increase in the oil recovery (Sheng, 2014).

Nanotechnology in EOR applications is one of the latest developments in reservoir engineering. Moreover, nanoparticles were speculated as good factors for solving reservoir engineering problems (Ogolo et al., 2012). Several studies showed that silica is the most used nanoparticle injection component; its role is to improve the EOR recovery mechanisms such as emulsion stability, wettability alteration, and IFT reduction. The main challenge of nanoparticles in EOR processes is stability in harsh conditions such as high salinity and high temperature (Azadgoleh et al., 2014).

EOR applications in carbonate reservoirs are challenging, owing to the reservoir water chemistry (divalent cations), the frequently high porosity but low permeability as well as

significant heterogeneity of carbonates. These processes include imbibition in the case of fractured reservoirs, wettability modification, and fluid-fluid interaction.

## 1.2 Scope and Overview

The study aims to clarify the role of nanomaterial application in terms of fluid-fluid interaction on a carbonate reservoir with low TAN oil. Also, to inspect the potential use of six different nanoparticle solutions for EOR applications and screening nanofluids potential, which is mainly evaluated by compatibility screening, phase behavior measurements, and interfacial tension IFT measurements.

# Chapter 2

## Fundamentals

This chapter handles the basic concepts which this work is trying to approach.

### 2.1 Enhanced Oil Recovery Principles

Oil production has three recovery stages: primary recovery, which by natural reservoir energy, secondary recovery by the supply of external energy to the reservoir that used injection fluids to increase reservoir pressure and increase recovery factor. Finally, tertiary recovery or enhanced oil recovery EOR is used for improving oil recovery and reduce residual oil saturation (Cheraghian & Hendraningrat, 2016). However, over time, the oil field's life during production leads to a decline in the reservoir pressure. Consequently, the reservoir energy cannot lift the oil onto the surface. Thus, water injection is a secondary recovery, and it is efficient to maintain the reservoir pressure and increase oil production. Water flooding was used as a secondary recovery, where water flooding injects directly to the reservoir in contrast to water injection injected in an aquifer. Water flooding has the same target as water injection, which was used to maintain the reservoir pressure and improve sweep oil. However, water flooding has an issue with heavy oil viscosity, which may lead to unstable displacement. Therefore, increase water flooding viscosity by adding some chemical agents or polymer to improve oil sweep efficiency (Beliveau, 2009).

After primary and secondary stages of production, enhanced oil recovery (EOR) became after that. EOR process uses to improving and increasing oil production in the reservoir, usually by injecting a substance into the oil reservoir to increase displacement and sweep efficiency of oil. Moreover, several different enhanced oil recovery methods, including Thermal recovery, gas, and chemical flooding (Gbadamosi et al., 2019).

However, chemical flooding is one of the EOR methods, and it has been widely used in several other industries. There are three kinds of chemicals involving alkaline, surfactant, and polymer, where each chemical has its unique functions and different mechanisms. Those mechanisms including improve the mobility ratio, decrease interfacial tension (IFT), and wettability alteration. Furthermore, alkaline such as sodium carbonate ( $\text{Na}_2\text{CO}_3$ ) react with crude oil to generate soap and increase pH. Furthermore, surfactant flooding is used to reduce interfacial tension (IFT) between oil and water, while polymer involves increasing water viscosity and improving sweep efficiency (Sheng, 2014).

## 2.2 Alkaline Flooding

### 2.2.1 Introduction

Alkaline flooding is one of the EOR techniques in which an alkaline solution such as sodium carbonate ( $\text{Na}_2\text{CO}_3$ ), sodium hydroxide (NaOH), or potassium hydroxide (KOH) is injected during water flooding or polymer flooding operations. An alkali is a base that dissolves in the water where the solution of a soluble base has a pH greater than 7 (Thomas et al., 2016). Furthermore, due to its cost-effectiveness, sodium carbonate ( $\text{Na}_2\text{CO}_3$ ) is the most widely used carbonate-based alkali lye (Leitenmüller & Rupprecht, 2019).

The alkaline chemical reacts with certain types of oils, the salinity of brine, and carbonate formations. When alkaline chemical reactions with acidic components in the crude oil phase led to creating in-situ surfactants, the reaction can reduce the interfacial tension IFT between oil and water and increase oil production. Also, it causes the formation of emulsions and changes in wettability (Samanta et al., 2011).

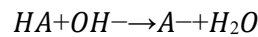
Alkaline flooding is believed to be controlled by three main mechanisms IFT reduction, wettability changes, and mobility control. IFT reduction occurs due to the generation of in situ surfactant in the oil, while wettability changes and mobility control due to oil emulsion and trapping. There is a parameter to consider when planning alkaline floodings, such as rock mineralogy, the number of organic acids present in the oil, and composition and compatibility of injection and formation water (Thomas et al., 2016).

### 2.2.2 Alkaline Reaction with Crude Oil

In alkaline flooding, the injected alkaline in oil reservoir causes reactions between alkaline and acid components in crude oil, leading to generating the formation of a soap, where this reaction occurs at the water/oil interface (Thomas et al., 2016).



The reaction equation is



where HA is a pseudo-acid component and A<sup>-</sup> is the soap component (Sheng, 2014).

The alkali-oil chemistry can be defined by acid component between the oleic and aqueous phases, and hydrolysis in alkali to produce a soluble anionic surfactant. A reaction enormously depends on the aqueous solution whence salinity and pH are shown in figure 2-1 (Sheng, 2013).

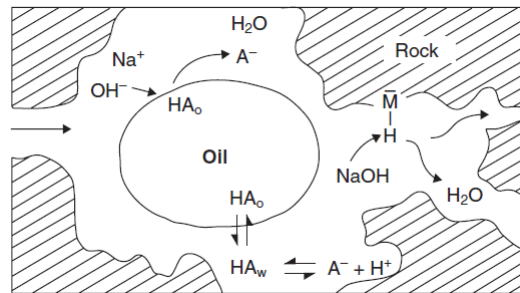


Figure 2-1: Schematic of the alkaline recovery process (deZabala et al., 1982).

Furthermore, organic acids in oil become ionized with add alkali while others stay electronically neutral. The interaction of hydrogen-bonding between the ionized and neutral acids, which causes create acid soaps (Sheng, 2013).

The critical parameter in this process is Total Acid Number (TAN). Total acid number (TAN) is a percentage of acid in oil according to standardized ASTM International that is determined by one gram of oil needed to neutralize with the amount of potassium hydroxide (KOH) in milligrams. It can be done via potentiometric titration, which works on the theory of electrical resistance. The unit of TAN is [mg KOH / g oil]. The application of alkaline flooding with high-TAN oil is usually more efficient (Park et al., 2017).

### 2.2.3 Alkali Interactions with Rock

The reaction between alkali and rock is considered the most difficult for alkaline flooding, where the number of reactions with alkalis is significant due to the complex mineralogy in reservoirs. The carbonate minerals have different types, such as limestone composed of calcium carbonate (CaCO<sub>3</sub>), and dolomite is an anhydrous carbonate mineral composed of calcium magnesium carbonate, CaMg (CO<sub>3</sub>)<sub>2</sub>. Also, anhydrite (CaSO) or gypsum (CaSO .2H<sub>2</sub>O) are considered highly undesirable due to all these minerals cause precipitations (Kumar et al., 1989).

For this reason, alkaline flooding is not recommended for carbonate reservoirs due to the abundance of calcium. The combination of alkaline chemicals and calcium ions can cause hydroxide precipitation that can damage the formation. The main issue of Alkali/rock reactions

is scaling and plugging in the producing wells and high caustic consumption (Kumar et al., 1989).

## 2.3 Phase Behavior

Phase behavior experiments play a significant role in understanding the performance of the interactive behavior of brine, alkaline, nanofluids, and crude oil. Also, phase behavior experiments aim to investigate the stability, optimal salinity, precipitation, optimal surfactant concentration, and oil type (Sheng, 2013). In general, phase behavior plays a vital role in the oil and gas industry, such as enhanced oil recovery compositional simulation, geochemical behavior, wellbore stability, geothermal energy, environmental cleanup, multiphase flow in wellbores and pipes, as well as surface facilities (Goodarzi & Zendehboudi, 2019).

The in-situ surfactant is generated when alkaline flooding reacts with crude oil, and hence the phase behavior between oil, brine, and surfactant is primary (Pal et al., 2018). Moreover, a surfactant (surface-active agent) is a chemical agent with the ability to adsorb onto the fluid/fluid interface. The surfactant molecule consists of two parts: a nonpolar (hydrocarbon) tail and an anionic/polar part called the head. Figure 2.2 shows the Schematic of the surfactant molecule. The tail is generally hydrophobic, which means that it is pushed due to its nonpolar nature out towards the oleic phase. In comparison, the polar heads tend to stay within the water phase.

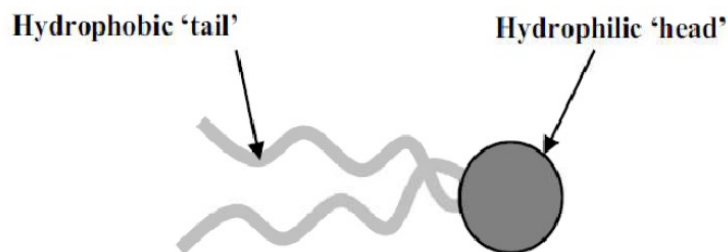


Figure 2-2: Schematic of the surfactant molecule (Chuo et al., 2014).

The main parameter that affects emulsion is the salinity of the brine. The increased brine salinity decreases the solubility of the anionic surfactant in the brine. It means that the surfactant is driven out from the brine as the concentration of electrolytes increases, and the surfactant moves from the aqueous to oleic phase (Pal et al., 2018).

The emulsion system consists of three types named macroemulsion, microemulsion, and nanoemulsion. First of all, macroemulsion are mixtures of two immiscible liquids with a droplet

size is larger than one  $\mu\text{m}$  (SHARMA & SHAH, 1985). The classification of macroemulsion is a single emulsion and double emulsion.

A single emulsion is an emulsion formed by two immiscible liquids, such as oil and water, where a surfactant film separates them to control the stability of dispersion and prevents droplets' coalescence. Based on which phase is dispersed into the other. It is divided into two categories, which are oil-in-water (O/W) or water-in-oil (W/O).

The double emulsion is an emulsion formed by two or more immiscible fluids separated by two or more emulsifier films. There are two types, which are O/W/O and W/O/W emulsions.

Secondly, the microemulsion is a mixture of two immiscible liquids and thermodynamically stable. Their droplet size does not exceed  $0.10\ \mu\text{m}$ . The classification of the microemulsion can be consist of three types, which suggested by Winsor in 1956. Winsor type II (-) is water external microemulsion which means that oil is soluble in water. Winsor type II(+) (Upper phase) is oil external microemulsion, water in oil emulsion. Finally, Winsor Type III is the middle phase or microemulsion bicontinuous microemulsion (Jeng & Miller, 1987).

Figure 2-3 shows the relationship between salinity and phase behavior. Moreover, the three microemulsion cases, exemplary ternary diagrams, and phase behavior are shown.

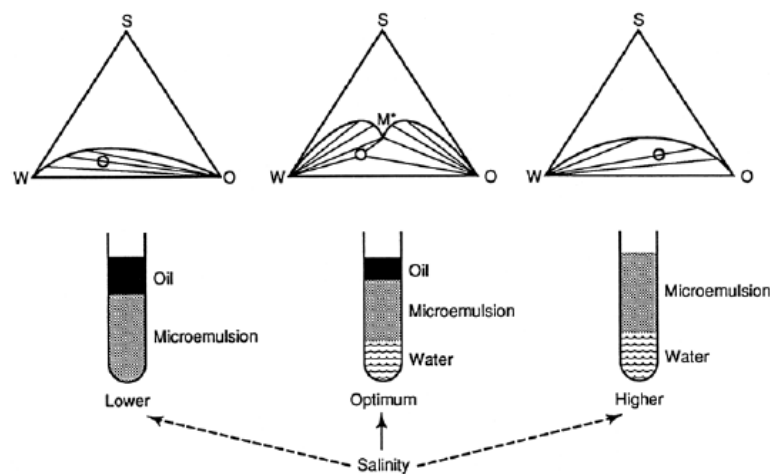


*Figure 2-3: Three Types of Microemulsion and the Effect of Salinity on Phase Behavior (Healy et al., 1975)*

Figure 2-3 illustrates how the brine's salinity affects phase behavior and how increasing salinity changes phase behavior. The optimum phase behavior is the microemulsion solubilizes equal amounts of oil and water. In this regard, the optimization of the phase behavior is dependent on the amount of salinity of the brine.

Finally, Nanoemulsions are small droplet size and stable colloidal systems. The system is very heterogeneous, and the droplet size ranges between 5 and 200nm (Aboofazeli, 2010).

However, Pickering emulsion is an emulsion that is stabilized by solid particles adsorbing at the water-oil interface, as shown in figure 2-4, where this type of emulsion was named after Pickering, who described them in 1907 (Yang et al., 2017). Pickering emulsions are considered of interest in many areas outside the oil industry field (Wang & Alvarado, 2008). Moreover, Arditty et al. (2004) reported that silica particles whose surfaces modified for change wettability could be used to stabilize oil in water emulsion by partially hydrophobized silica or water in oil-emulsion via hydrophobized silica. Several factors impact Pickering emulsions' stability, namely composition of the oleic phase, the salinity of the brine phase, pH of the aqueous phase, and temperature (Wang & Alvarado, 2008).

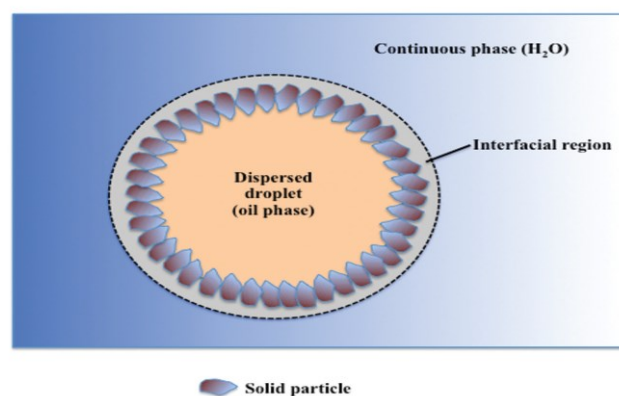


Figure 2-4 Pickering emulsion (Mcmullen & Ingredients, 2014).

## 2.4 Interfacial Tension, IFT

Interfacial tension is a force per unit length of two immiscible fluids, while the force of air and liquid interface is often referred to as surface tension. The unit of the interfacial tension is milli-Newtons per meter (mN/m) or dynes per centimeter (dyne/cm), wherein in literature, the symbol is often given as  $\gamma$  or  $\sigma$ . There are parameters effect on of interfacial tension such as the composition of the oil and water phases, temperature, and minor by the pressure. According to the study Hassan et al. (1953), they found the IFT effect by temperature, with increasing temperature, the IFT decreases.

### 2.4.1 IFT Measurement Methods

The methods to measure interfacial tension, namely the pendant drop, Du Noüy ring, and spinning drop tensiometer. The techniques such as pendant drop and Du Noüy ring measure for high IFT, which is more than  $10^{-1}$  mN/m. On the other hand, the spinning drop tensiometer is considered the most well-known technique for measuring low IFT, approximately  $10^{-2}$  mN/m and lower. The spinning drop technique for measuring interfacial tensions between two immiscible fluids by the rotation of a vessel at a defined rotational speed was suggested in 1941

by Vonnegut (Vonnegut, 1942). Consequently, the spinning drop measurement has two methods available, named the Young–Laplace and Vonnegut. Both methods depend on the shape of the oil droplet (Viades-Trejo & Gracia-Fadrique, 2007).

Figure 2-5 illustrates that a small droplet of liquid (A) is a light liquid such as crude oil suspended in a heavy liquid such as solution (B) is put under rotation about a horizontal axis. To reach an equilibrium position, the centrifugal forces oil droplet (A) will move to the middle forming a drop astride the spinning axis as the centrifugal force rises to a high enough value, the drop shifts to a cylindrical form. The elongation of the oil droplet stops when the centrifugal forces are balanced by the interfacial tension forces, where the length of the droplet is large compared with the radius ( $L \gg R$ ) (Viades-Trejo & Gracia-Fadrique, 2007).

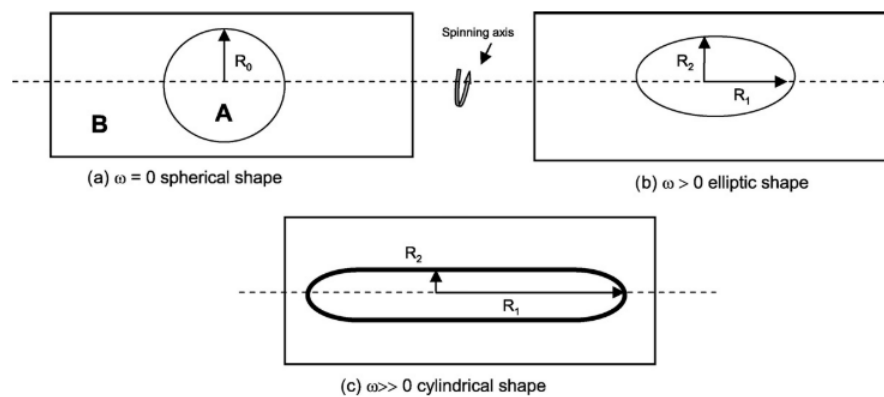


Figure 2-5 Spinning drop method (Viades-Trejo & Gracia-Fadrique, 2007)

By suggested Vonnegut (1942), the interfacial tensions are calculated using Eq

$$\sigma = \frac{\Delta\rho\omega^2}{4} R^3$$

Where,

$\sigma$  – Interfacial tension [N/m]

$\Delta\rho$  – density difference [kg/m<sup>3</sup>]

$\omega$  – rotational speed [rad/s]

$R$  – radii of curvature [m]

However, with the Young–Laplace method, it is possible to calculate the interfacial tensions IFT which expression for spherical shape. Mathematically, it can be represented by

$$\Delta P = \sigma \left( \frac{1}{R_1} + \frac{1}{R_2} \right)$$

$\Delta P$  is the pressure difference between phases,  $\sigma$  is interfacial tensions, and  $R$  is the sphere radius.

Moreover, figure 2-6 below illustrates the types of droplet shapes based on an interfacial tension value between fluids. Since the drop is elongated, it means that IFT between two immiscible fluids is very low. In contrast, when interfacial tension is high, the droplet of fluid will take a spherical shape.

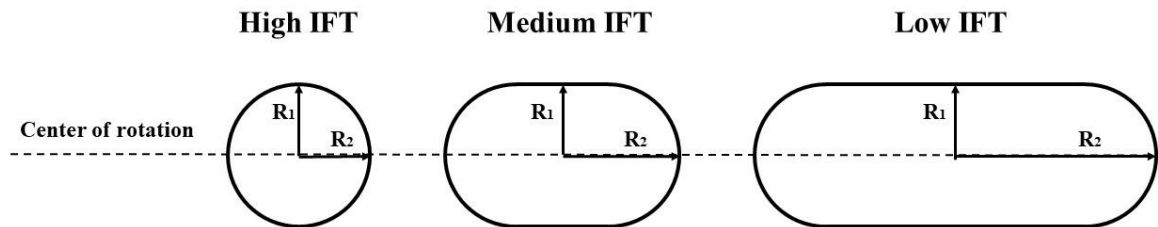


Figure 2-6: Shape of spinning drop related to interfacial tension (Arekhov, 2019)

### 2.4.2 IFT and Oil Recovery

The oil recovery is directly related to capillary number  $N_{ca}$ . A capillary number is a dimensionless number which is defined as the ratio of viscous over capillary forces (Kamal et al., 2017). Mathematically, it can be represented by

$$N_{ca} = \frac{\text{Viscous forces}}{\text{Capillary forces}} = \frac{V \times \mu}{\sigma \cos\theta}$$

Where  $v$  is the velocity,  $\mu$  is the dynamic viscosity,  $\sigma$  indicates the IFT, and  $\theta$  is the contact angle.

In order to improve oil recovery and reduce residual oil saturation, a higher capillary number is essential. To obtain a higher capillary number, IFT must be decreased to an ultra-low value, as illustrated in the equation. Therefore, the capillary number increases are considered one of the EOR process goals (Guo et al., 2017).

The observed standard errors may cause uncertainty of measurement for the following reasons:

- a) The junction of multiple oil droplets causes a change in dimensions, and thus IFT measurement gives a new value.
- b) The camera stopped connection occasionally, which in results missing data, and hence the camera was set up again.
- c) Change the fitting algorithm when measuring based on drop shape.

Interfacial tension of more than one mN/m is more suitable to use the pendant drop method and Young-Laplace as algorithms. In contrast, for low IFT systems below one mN/m is better to use the Spinning drop method and Vonnegut as algorithms due to the oil droplet shape.

# Chapter 3

## State of the Art

### 3.1 Nanotechnology

#### 3.1.1 Historical Overview

Nanotechnology has provided a means of entrance interest the recent years in the oil and gas industry. Nanoparticles are small particles with a diameter of 1-100 nm, and they have special unique properties because of their small sizes (Singh & Ahmed, 2010). In addition, different studies have shown that nanoparticles have promising roles in enhanced oil recovery, particularly the silica-based NPs, because of their ability to alter wettability and reduce the interfacial tension (IFT) and improve the mobility ratio (Kamal et al., 2017). In addition to their roles in recovery enhancement mechanisms, nanoparticles have the ability to pass easily through the pore throats in the porous media due to their small sizes can also stay dispersed within the solutions due to their active surface high stability (Cheraghian & Hendraningrat, 2016).

Over the last decade, many studies have shown that nanoparticles provide promise for potential EOR processes where silica-based NPs are most widely used. Even though the mechanism for oil displacement through NPs is not yet understood, nanotechnology is chosen as an alternative method for unlocking the remaining oil resources and implemented in the last decade as a new EOR method (Cheraghian & Hendraningrat, 2016).

#### 3.1.2 Types of Nanoparticles

Nanoparticles can be classified based on the composition of their constructing units, which are metal oxide, organic, and inorganic. The nanoparticle has different types such as silica oxide  $\text{SiO}_2$ , aluminum oxide  $\text{AlO}_3$ , iron oxide  $\text{Fe}_2\text{O}_3$ , Zirconium dioxide  $\text{ZrO}_2$ , Titanium dioxide  $\text{TiO}_2$ ,

and Tin (II) oxide SnO. Those types of nanoparticles have a substantial impact on reducing IFT between water and oil, where increase NPs concentration leads to reducing IFT. Besides, silica oxide is considered the most effective on IFT compared to other types of nanoparticles. The surface nanoparticle can be modified to reduce IFT, change wettability, and improve oil recovery (Kamal et al., 2017).

### 3.1.3 EOR with NP Assistance

Nanotechnology has several abilities used in the oil and gas industry to solve various problems. Due to their ability to modify specific properties in formation, nanoparticles (NPs) were used in sub-surface applications. Consequently, adding NPs to the fluids leads to boost the nanofluid mechanism to be more efficient in enhanced oil recovery via wettability alteration and reducing residual oil saturation. Nanofluid can also provide formation damage treatment while strengthening sand consolidation, removing asphaltene damage, and increasing the mobility of the capillary- trapped oil (Cheraghian et al., 2014).

The nanofluid EOR mechanisms are essential to understand when NPs are used as novel EOR agents for nano assist EOR process as shown in figure 3-1. These mechanisms include IFT reduction, wettability alteration, disjoining pressure, preventing asphaltene precipitation, as well as pore channels plugging, and decreasing the mobility ratio (Sun et al., 2017).

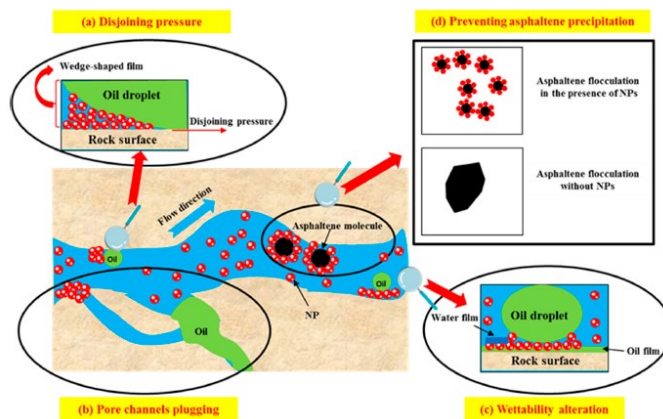


Figure 3-1 The schematic of nanofluids mechanisms (Sun et al., 2017).

## 3.2 Stability of Nanofluid

The stability of nanofluids is a challenging issue. It is essential to analyze factors influencing nanofluids' dispersion stability because the stability of NPs is a vital issue that influences the properties of nanofluids for application. There are many methods to evaluate the stability of nanofluids. The simplest method is visual observation (Yu & Xie, 2012).



Furthermore, Zeta potential is the electrical potential at the slipping plane and can use it to predict the particles' long-term stability. Therefore, the high Zeta potential, either negative or positive, indicates the stability of NPs while at low Zeta potential tend to coagulate or aggregation. In general, a value of 10 mV, either negative or positive, is believed to be excellent aggregation, while more than 60 mV tends to higher stability (Yu & Xie, 2012).

The DLVO theory is describing the stability of colloids in suspension, such as nanoparticles dispersed in water. Also, this theory describes the interaction between two NPs based on their distance. DLVO was named (Arreguin, Landau, Verwey, and Overbeek).

The DLVO theory mainly concerns the balance between two forces: electrostatic repulsion and van der Waals attraction. The attraction of Van der Waals is the result of forces in each colloid between individual molecules. Thus, it is essential to keep each particle discrete and avoid them from gathering agglomeration by maximizing the repulsive forces by increasing surface charge between particles (Hendraningrat & Torsæter, 2014). The surface charge state can be measured using zeta potential.

The electrostatic repulsion between the particles is an essential mechanism for nanoparticle dispersion stability (Huh, et al., 2019). Furthermore, when the repulsion forces are stronger than the attractive force, the attraction force tends to overpower the repulsion, the particles then bind to each other, and final sedimentation occurs (Mohamed et al., 2018). The two types of repulsion that affect colloidal stability are divided into two kinds: steric repulsion and electrostatic repulsion.

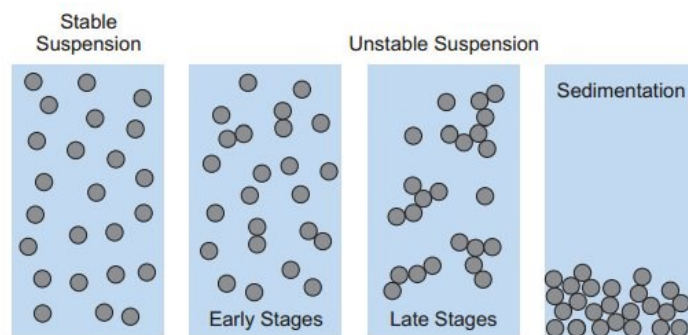


Figure 3-2 stable and unstable suspension (Mohamed et al., 2018).

According to Li et al. (2020), nanoparticles' stability uses surface or chemical modification and without it. They observed that nanofluid with surface modified had the best stability, while nanofluid without surface-modified had the worst stability. All samples were agglomerated and settled within one day.

However, the reservoir's environment, including temperature, salinity, pH, and chemical and physical nature of the reservoir rock, such as surface charge, has a significant influence on the

fate of NPs in a reservoir. In this part, the two factors that affect NPs stability, which is salinity and temperature, are detailed below.

### 3.2.1 Impact Salinity on NPs Stability

The stability of NPs dispersions in aqueous solutions strongly depends on electrostatic repulsion force between the same charged surfaces of nanoparticles. The presence of salts acts on shrinks and compresses the electrostatic double-layers size, which causes a sharp reduction in the electrical repulsion force between the NPs. Furthermore, high salinity leads to unstable nanoparticles and causes coiled aggregation due to the leak of electrostatic repulsion force between nanoparticles (Alnarabiji & Husein, 2020).

Ionic strength (I) of the liquid phase is considered one of the disadvantages of NPs suspensions stabilized through electrostatic. As ionic strengths decrease, the double layer's thickness is around 5-10 nm, which is the order of the van der Waals forces' distance of interaction. Thus, because of the dominant effect of repulsive forces, the NP suspension is stable. On the other hand, the double layer thickness is reduced, and the ionic strengths increase, and hence NPs tend to aggregate in a brine (Huh et al., 2019).

Metin et al. (2011) studied the effect of divalent cations of the formation brine such as  $\text{Ca}^{2+}$  and  $\text{Mg}^{+2}$  on nanofluids. They observed that divalent cations are more practical to destabilize silica nanoparticle dispersion than monovalent  $\text{Na}^+$ .  $\text{Mg}^{+2}$  is the most effective in destabilizing silica nanoparticles. Mahmoudi et al. (2019) reported that salinity NaCl decreases the stability of silica nanoparticle solutions. After adding the surfactant, the stability of the silica nanoparticle increase.

### 3.2.2 Impact of Temperature on NPs Stability

The temperature is considered one of the main factors that affect the stability of nanoparticles. The nanofluid stability reduces when the temperature increase and the kinetic energy of particles increase as the temperature rises. Thus, this promotes successful particle collision and aggregation. The increasing nanoparticle concentration leads to decreases in solutions' stability (Mahmoudi et al., 2019). Metin et al. (2011) reported a similar influence of temperature on the stability of silica nanoparticles. They found that the aggregation rate is increased by increasing temperature from 25°C to 70°C.

## 3.3 Influence of NPs on IFT

Nanofluid plays a significant role in affecting Interfacial tension (IFT). One of the NPs mechanisms is reducing IFT alone or in combination with surfactant between oil and water.

According to Joonaki and Ghanaatian (2014) study. They found that most NPs have more efficient in reducing IFT, which is silica oxide  $\text{SiO}_2$ , compared to other types of NPs. Besides, the other types of NPs such as aluminum oxide  $\text{AlO}_3$ , iron oxide  $\text{Fe}_2\text{O}_3$ , and Titanium dioxide  $\text{TiO}_2$  also affect IFT reduction.

The main reason for the IFT reduction is adsorption NPs at the oil-water interface. Therefore, nanoparticles must adsorb on the oil-water interface. Thus, the adsorption of NPs has two main mechanisms, namely Langmuir monolayer and Gibbs monolayers (Sofla et al., 2019). Moreover, the smaller the nanomaterial size has higher catalytic activity, the greater their Brownian motion and higher thermal conductivity in water (Kim et al., 2016) Therefore, smaller particles have higher adsorbed at the oil and water interface.

Numerous research investigated the IFT reduction caused by NPs. Wei et al. (2016) Observed that increasing the concentration of nanocellulose above 0.8% did not decrease IFT. Sofla et al. (2019) reported that pressure has not affected the performance of silica nanoparticles. Neubauer et al. (2020 a) furthered to compare the ability of two types of nanofluids (surface-modified silicon dioxide nanoparticles, whereas the other utilizes surface-modified silicon-dioxide nanoparticles, surfactants, and solvents) to reduce IFT in low and high total acid number TAN oil. They observed that IFT for the nanofluid that contains surface-modified silicon dioxide was reduced in brine/ low TAN oil system from 5.9 mN/m to 0.8 mN/m. In contrast, the other nanofluid contains surfactant and solvent, IFT reduces from 5.9 mN/m to 0.5 mN/m, as shown in figure 2-3. The results illustrate that IFT reduction between nanofluids and oil is not affected by the oil acidity.

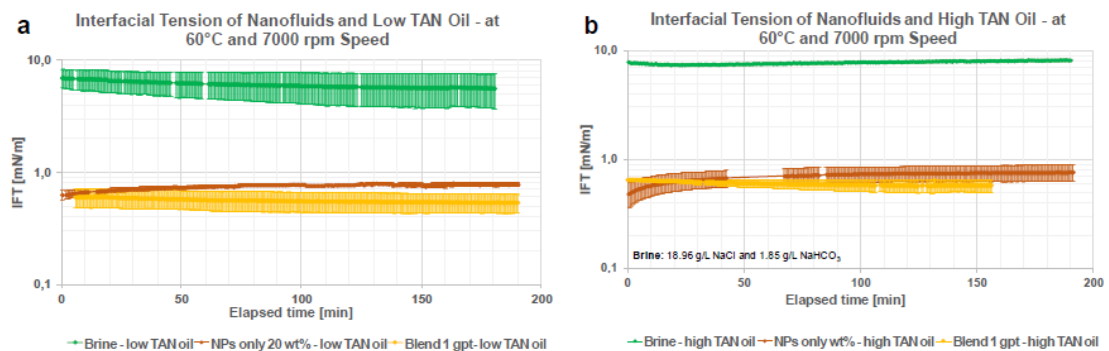


Figure 3-3 IFT measurements at 60°C and 7000 rpm (a) between low TAN crude oil and brine (b) IFT measurements between high TAN crude oil and brine (Neubauer et al., 2020 a)

Ma et al. (2008) investigated the effect of silica oxide NPs with cationic, anionic, and nonionic surfactant on IFT. The authors found that the cationic surfactant could change the surface of silica oxide NPs from fully hydrophilic to partially hydrophobic. This change boosts the aggregation of NPs, leading to reducing IFT. Moreover, they detected the efficacy of anionic

surfactant is improved to minimize IFT by adding hydrophilic silicon oxide NPs. In contrast, the performance of nonionic surfactants has not been influenced by hydrophilic silicon oxide NPs.

Furthermore, the concentration of surfactant and NPs are a key factor that affects the IFT. According to Ma et al. (2008), using silica oxide  $\text{SiO}_2$  NPs in the presence of surfactant to examine the effect on IFT. As a result, they found that IFT decreases at a low concentration of NPs and surfactants. In contrast, increase NPs concentration leads to increase IFT. The main reason behind this is the electrostatic repulsive interactions between the anionic surfactant and NPs which means the increased add of NPs to surfactant leads to the surfactant's diffusion towards the interface. Moreover, the NPs can carry surfactant molecules towards the interface, but at a high concentration of NPs, NPs prevent surfactant molecules toward the interface (Ma et al., 2008).

Another research by Neubauer et al. (2020 b) studied the effect of the nanofluids and alkaline on interfacial tension reduction. They found that IFT reduction is strongly dependent on the surface charge and the size of the nanomaterials. The more negatively charged silica NPs were more effective in IFT reduction than neutrally charged silica. On the other hand, nanomaterial with a smaller size has the lowest IFT reduction, even though it has neutrally charged nanomaterial, as shown in figure 3-4. As particle size decreases, the number of particles in a volume unit of nanofluid increases. Hence, the number of particles that accumulate at the oil/water interface leads to reduced IFT.

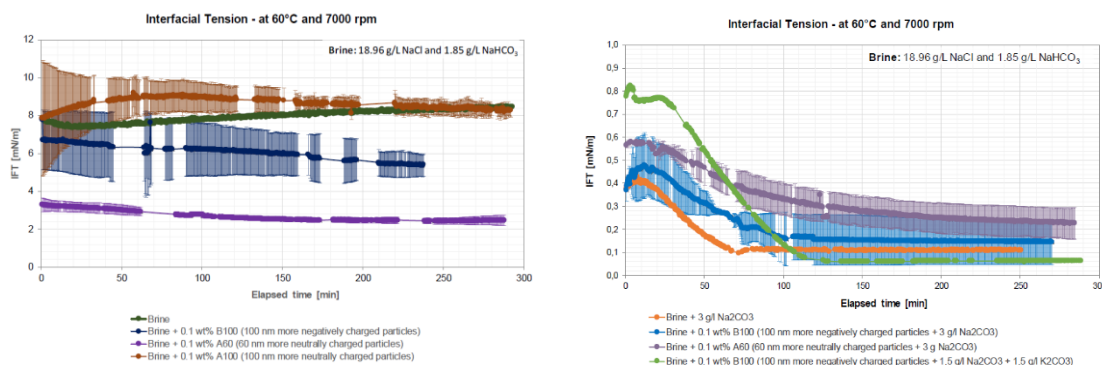


Figure 3-4: IFT measurements between crude oil and brine/nanofluids (Neubauer et al., 2020 b)

Dahkaee et al. (2019) studied the effect of nanofluids with different salinity on ultra-interfacial tension reduction. They found that  $\text{NiO/SiO}_2$  nanoparticles together have lower IFT than  $\text{NiO}$  or  $\text{SiO}_2$  when used alone, while  $\text{SiO}_2$  alkaline has the lowest IFT compared to other NPs. Moreover, the results show that the effect of salinity with different concentrations of divalent cation  $\text{Ca}^{+2}$  and  $\text{Mg}^{+2}$  does not affect most nanofluids' performance. Therefore, the salinity has a positive effect on nanofluids' performance to reduce IFT (Dahkaee et al., 2019). Moreover,

Esmailzadeh et al. (2014) reported the impact of nanoparticle  $ZrO_2$  on interfacial properties with an anionic surfactant. They found that  $ZrO_2$  nanoparticles lead to an increase in the anionic surfactant's surface activity and a reduction in IFT between water and oil.

Jalil and Hussein (2019) reported silica oxide nanoparticles' influence with different sizes 52, 65, and 5nm and different concentrations on Interfacial Tension. They found that all nanoparticles' size has almost the same influence on oil-water interfacial tension reduction, and increased concentration led to reducing IFT, as shown in figure 3-5. Besides, reducing interfacial tension increasing the capillary number, and hence a higher capillary number causes an increase in oil displacement efficiency (Jalil & Hussein, 2019).

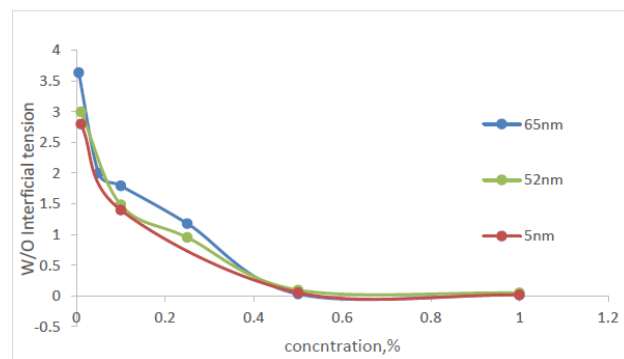


Figure 3-5 interfacial tension W/O versus silica with different size of NPS (Jalil & Hussein, 2019)

Hosseini et al. (2015) reported the effect of divalent cations ( $Ca^{2+}$  and  $Mg^{2+}$ ) on IFT. They observed that the increase in divalent cations in brine reduces IFT in the presence of cationic surfactant. The main reason is that the same electric charge of the divalent cations increases the cationic surfactant's electric charge, leading to compressing the interfacial double layer. Therefore, surfactant molecules could enter the micelle to enlarge the radius of the micelle particle by increasing the repulsion between surfactant molecules, which results in reduced IFT.

### 3.4 Effect of Nanoparticles on Stabilized Oil/Water Emulsion

Alkali flooding depends on the chemical reaction to generate in-situ surfactants between compounds such as sodium or potassium carbonate and organic acids in crude oil. The in-situ surfactant settles at the oil-water interface, reduces the interfacial tension (IFT), and creates an emulsion (Sheng, 2015). Moreover, the generated emulsions can act as flow barriers to divert the flow into unswept zones and block high permeable channels.

The emulsion of oil-in-water has a higher viscosity than water, but it is also less viscous than oil. The distribution of slug-wise viscosity can help realize flow conformity between the phases and a stable piston-like displacement. Furthermore, the emulsion-assisted mobility control is

not maintained, and the emulsion is not stable enough during the flooding to withstand the driving force. Hence, and the oil improvement will be only temporary (Bryan et al., 2013).

However, Nanoparticles can use as emulsion stabilizers and alternatives to surfactants. The stability and ability of nanoparticles to resist harsh environments are very strong. NPs can augment emulsion stability by accumulating and adsorption on the interface between two immiscible fluids (Divandari et al., 2020), where this type of emulsion is called Pickering emulsion. Nevertheless, the type of nanomaterial surface modification had a weak effect on the stabilized volume of the emulsion (Neubauer et al., 2020 b).

Several factors impact the stability of Pickering emulsions, namely composition of the oleic phase, the salinity of the brine phase, pH of the aqueous phase, and temperature (Wang & Alvarado, 2008). The oleic phase composition includes asphaltene precipitation, where asphaltene plays an essential role in the stability of crude oil emulsions.

NPs have the potential to decrease surfactant adsorption on the reservoir rock surface. Zargartalebi et al. (2015) studied showed that using additional NPs to surfactant lead to reduce surfactant adsorption on the rock surface. Also, the surfactant adsorption decrease compared to surfactant solution without NPs. Furthermore, Sheng (2015) reported the effect of Alkali to react with low and high TAN crude oil. They observed that low acid components could not produce soap compared to high acid components with some emulsion volume.

Neubauer et al. (2020 b) investigated silica NPs to boost the stability emulsions created by alkali-polymer to find the optimum long-lived emulsion stabilize. They observed that there was no emulsion when silica nanomaterials at different types and concentrations were used. There was emulsion when adding Silica NPs to alkaline in the solution. The emulsion volume was stabilized even add the polymer to a solution.

Grutters et al. (2007) conducted experiments to assess the role of asphalts in stabilizing W / O emulsions in crude oil with 20 API°. They disagree that the observed loss of stability could be attributed to the reduced viscosity of the continuous phase when precipitating asphaltene. Furthermore, they also point out that polar resins, such as naphthenic acids, play a significant role in their experiments in stabilizing the emulsions.

Wang and Alvarado (2008) studied the effect of salinity and pH on Pickering emulsion stability. They use different salinity with 1, 10, and 100 times dilution was emulsified with crude oils. They found that low-salinity conditions promote the formation of stable water-in-oil emulsions. Also, silica-stabilised emulsions' results indicate that larger silica particles are more stabilizing than smaller silica particles. This result due to the stabilizing steric repulsion.

# Chapter 4

## Experimental Setup and Materials

### 4.1 Fluid Preparation and Characterization

The first step in this work is to prepare the fluids. Synthetic brines were used. One mimics the real composition of the brine of a Romanian carbonate reservoir, while the other mimics the composition of softened brine. Besides, six types of nanofluids and sodium carbonate  $\text{Na}_2\text{CO}_3$  as alkali were used. Crude oil from the Romanian carbonate reservoir was used for fluid-fluid interaction experiments.

#### 4.1.1 Brine Composition

The brine composition plays an essential role in the potential application of nanofluid and alkali flooding processes. Two synthetic brines were prepared to investigate the chemical compatibility, IFT, fluid characterization, and phase behavior experiments. The first synthetic brine is called real brine, where real brine represents the composition from the OMV's carbonate reservoir and has a high concentration of divalent cations, as shown in table 4-1. Besides, the real brine was used to mimic the salinity and buffering capacity of the reservoir water. The second type of synthetic brine is softened brine. The softened brine contains low concentrations of divalent cations such as calcium, and it does not have magnesium compared to real brine, as shown in table 4-2.

The main properties and composition of the brines are shown in tables 4-1 and 4-2

Table 4-1 Synthetic formation brine

Real Brine Compounds	[mg/l]
NaCl	64200
KCl	550
MgCl <sub>2</sub> *6H <sub>2</sub> O	7800
CaCl <sub>2</sub> *2H <sub>2</sub> O	10700
Na <sub>2</sub> SO <sub>4</sub>	930

Table 4-2 Soften brine composition

Softened Brine Compounds	[mg/l]
NaCl	64000
KCl	150
CaCl <sub>2</sub> *2H <sub>2</sub> O	40*
Na <sub>2</sub> SO <sub>4</sub>	700

\*equivalent to 11 mg/l Ca<sup>2+</sup> as a sum of all divalent cations

Some devices, tools, and minerals were used to prepare synthetic formation brine and softened brine, namely digital balance scale, funnel, spoon, papers, filter paper, deionized water.

The steps to prepare a synthetic real brine and softened brine as following:

1. Prepare quantities of salts such as NaCl, Na<sub>2</sub>SO<sub>4</sub>, MgCl<sub>2</sub>\*6H<sub>2</sub>O, CaCl<sub>2</sub>\*2H<sub>2</sub>O, and KCl according to the composition and properties of formation brine in the Romanian field as shown in table 4-1. Subsequently, deionized water was mixed with these minerals to prepare 10 liters of synthetic formation brine.
2. Softened brine was prepared by mixing specific amounts of NaCl, Na<sub>2</sub>SO<sub>4</sub>, CaCl<sub>2</sub>\*2H<sub>2</sub>O, and KCl shown in table 4-2 with deionized water to prepare 10 liters.
3. After preparing synthetic real and softened brines, they were filtered using filter paper with size 40 μm to remove small salt particles.

However, the workflow to prepare synthetic brine in the lab is shown in Figure 4-1.



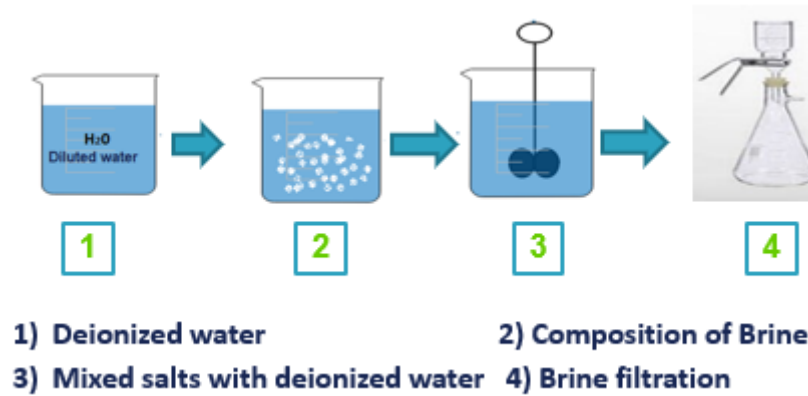


Figure 4-1 The steps process to prepare syntactic brine

### 4.1.2 Crude Oil

The OMV's reservoir crude oil was used in this work for all tests without further treatment. It is a light oil and with a density is  $0.796 \text{ g/cm}^3$  ( $46^\circ\text{API}$ ) at reservoir temperature ( $73^\circ\text{C}$ ) and  $0.83 \text{ g/cm}^3$  ( $39^\circ\text{API}$ ) at  $25^\circ\text{C}$ . The total acid number (TAN) of the crude oil is about  $0.13 \text{ mg KOH/g}$ , measured by titration. Viscosity at current reservoir conditions (pressure  $158 \text{ bar}$ ) is  $1.87 \text{ mPa.s}$ , and  $5.48 \text{ mPa.s}$  at  $25^\circ\text{C}$  (pressure  $1 \text{ bar}$ ). The properties of crude oil samples are shown in table 4-3 below.

Table 4-3 Properties of crude oil samples

Crude oil	OMV carbonate reservoir
TAN [mg KOH/g]	0.13
Saturates %	60.3
Aromatics [%]	26.6
Resins [%]	11.9
Asphaltene [%]	1.1
$\mu$ @ $73^\circ\text{C}$ [cP]	1.87
$\rho$ @ $73^\circ\text{C}$ [ $\text{g/cm}^3$ ]	0.830

### 4.1.3 Nano Fluids

Six types of Nanofluids were used: nanofluid (S1), nanofluid (R1), E100, P100, and nanofluid A1& A2. The nanofluids used employ inorganic nano-sized particles, and

some of them are dispersed in other chemical compounds such as surfactants and solvents.

Nanofluid (S1) is using nano-sized particles in a colloidal dispersion. It is designed to improve oil recovery and reduce IFT. Such particles act as a wedge film driven by Brownian motion and diffusion described as disjoining pressure, which significantly promotes and accelerates the movement of gas, oil, and water, or their mixture (Wasan et al., 2011).

Moreover, nanofluid (S1) can apply in high temperatures up to 175 °C nanofluids (S1) can be made fluid compatible formulations in low, neutral, and high pH. Nanofluid (S1) contains silicon dioxide (SiO<sub>2</sub>) that can change wettability from oil-wet to water-wet in carbonate reservoirs.

The second type of nanofluid is nanofluid (R1) contains silicon dioxide SiO<sub>2</sub>, surfactant, and solvents. Nanofluid (R1) is designed to improve oil recovery and provides unique advantages in terms of diffusion, interfacial tension reduction, fragmentation, and disjoining pressure. Besides, it enhances fluid stimulation interaction in the fracture face, leading to increased oil and gas production (Boyle, 2016).

The surfactant present in nanofluid (R1) reduces the interfacial tension (IFT) in the reservoir and mobilizes immobile water-block areas in pore spaces. Simultaneously, the solvent reduces oil viscosity through solvent miscibility with the oil, which leads to improving the mobility ratio (Boyle, 2016).

Two types of nanomaterials named E100 and P100 were also used. The particle size d<sub>50</sub> derived from the dynamic light scattering of E100 and P100 materials are 106 and 114 nm, respectively, where E100 and P100 stem from the same base material. The physical and chemical properties of the nanomaterial stock solutions are shown in table 4-4.

The key distinctions between nanomaterials E100 and P100 are surface functionalization. The surface modification of the P100 results in a more neutral surface charge, while the E100 sample results in a more negative surface charge.

*Table 4-4: Physical and chemical properties of the nanomaterial stock solutions.*

	nanoparticle type	Solid content [%]	Viscosity [mPa.s]	Particle size [nm]	pH
E100	SiO <sub>2</sub>	27.9	39.0	114	3.2
P100	SiO <sub>2</sub>	22.5	16	106	9.5

Nanofluid A1 and A2 are a proprietary solution consisting of water, nanoparticles, surfactants, and other additives designed to enhance water wettability over a long period. The nanoparticles of A1 and A2 are contained aluminum oxide  $\text{Al}_2\text{O}_3$  and silicon oxide  $\text{SiO}_2$  with different surface modifications.

The composition of Nanofluid is a trade secret, and the process by which nanoparticles stay stable in solution is the subject of a patent application. The solution can be handled safely and is nontoxic. The concentration of nanofluids was recommended for OMV field applications.

## 4.2 Compatibility Test

The compatibility was tested to investigate which alkali and nanofluids concentrations are compatible with both synthetic formation brine and softened brine. In this experiment, six nanofluids were used, namely S1, R1, E100, P100, A1 and A2, at different concentrations. Also, the alkali solution used in this experiment was sodium carbonate  $\text{Na}_2\text{CO}_3$ . One of the parameters that need to be tested ahead of alkali flooding is the composition and compatibility of injection water and formation brine. For this reason, it is necessary to do a compatibility test.

The compatibility test was performed using a 20 ml borosilicate glass bottle. All fluid samples were poured into the borosilicate glass bottle using tools of preparation samples such as Eppendorf, pipettes, and digital weight scale. The steps of the preparation compatibility test as following:

1. Preparation of sodium carbonate  $\text{Na}_2\text{CO}_3$  in real brine at two different concentrations, 10 & 20 g/l.
2. 20 ml of the respective alkali solutions were prepared by mixing alkaline and softened brine. The alkaline solution concentrations ranged from 1000 to 10,000 ppm, as shown in figure 4-3.
3. Nanofluid (S1) was prepared at 10 wt%, 15 wt%, 20 wt%, 25 wt%, and 30 wt%. Nanofluid (S1) was mixed with softened and syntactic formation brine, as shown in figure 4-4.
4. Nanofluid (R1) was prepared with real and softened brine at concentrations of 1 gallon per thousand (1gpt) and 2 gpt according to company product recommendations.
5. E100 and P100 were prepared with real and softened brine at concentrations of 0.1 wt%, as shown in figure 4-5 (Neubauer et al. 2020).
6. Nanofluid A1 & A2 were prepared with real and softened brine at two concentrations which are 10 & 20 wt%, as shown in figure 4-6.

After preparing nanofluids and alkali solutions with different concentrations, all samples were put together and sitting in the oven under reservoir temperature condition, which is  $73^\circ\text{C}$  for a week, where gathered pictures and observations. The compatibility test process was taking

several days where it divided into two parts are the first part is the first day at room temperature, and the second part is after 24 hours, and one week under 73°C.



Figure 4-2 Eppendorf and pipettes



Figure 4-3 Alkaline solution (softened brine) at different concentrations



Figure 4-4 Nanofluid (SI) at different concentrations for real and softened

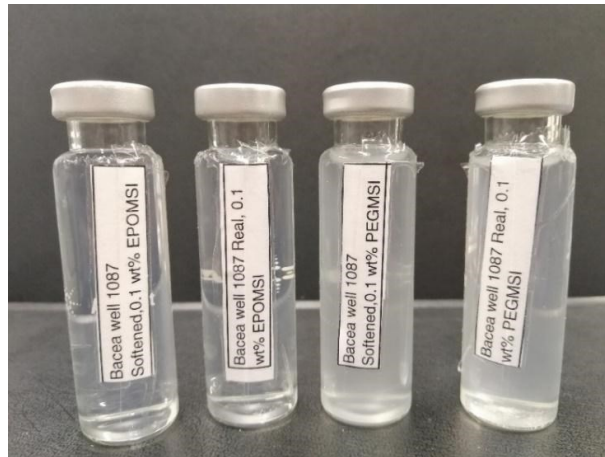


Figure 4-5 Nanofluid (P100 & E100) for real and softened



Figure 4-6 Nanofluid (A1 & A2) at different concentration for real and softened

### 4.3 Phase Behavior Experiments

Phase behavior experiments play a significant role in understanding the interactive behavior of brine, alkaline, nanofluids, and crude oil. The phase behavior experiments were assessed using the procedure described by Sheng 2011. Furthermore, phase behavior studies were performed to assess the potential of each nanofluid and alkali solution sample at the salinity and temperature of the OMV oil field.

Phase experiments were carried out using 10 ml of borosilicate pipettes which were sealed with an oxygenated methane torch at the bottom. The transparent glass pipettes enabled visualization of emulsion stability by monitoring the interface position between oil, emulsion, and the water phase. The pipette was fitted with equivalent volumes of aqueous and oil phase (5 mL/5mL), giving a ratio of 5:5. The desired aqueous solution was prepared directly in the pipette, using an Eppendorf pipette to add amounts of alkali stock solution at different concentrations and

nanofluids suspensions such as S1, R1, P100 & E100, and nanofluid A1 & A2 at different concentrations. The concentration of nanofluids used in the experiments was recommended by OMV, as shown in Table 4-5 below. The concentration of the alkaline solution was ranging from 1000 to 10,000 ppm.

Table 4-5 The values of concentrations for Nanofluids

Chemical blends		
Nanofluids	Types	Concentration [wt%]
	NP S1	10, 15, 20, 25, 30
	NP R1	1 & 2 gpt
	P100	0.1
	E100	0.1
	A1	10, 20
	A2	10, 20

A syringe was used to pour 5 ml of crude oil into the pipettes. At ambient temperature, the tops of the borosilicate pipettes were sealed and left aside to cool. Sealed pipettes were then shaking for 64 hours or 90 hours in a rotator mixer. The workflow of phase behavior was shown in figure 4-7. Finally, pipettes were kept at 73°C in convection ovens. Table 4-4 presents the tested possible combinations for the phase behavior experiments, of which 36 combinations in total are included in this work. All experiments were made in triplicate.

Furthermore, in phase behavior experiments, the volume of the oil phase, emulsion, and aqueous phase were determined by a graduated pipette.

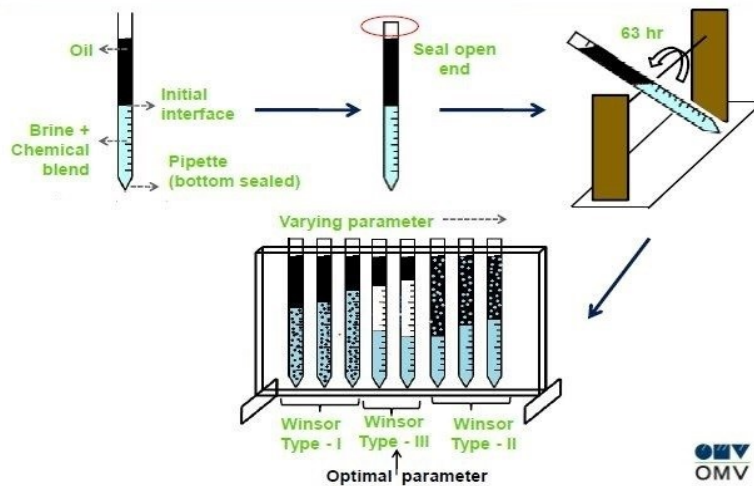


Figure 4-7 The workflow of a phase behavior experiment

## 4.4 Density and Viscosity Evaluation

In order to define the properties of the material, such as dynamic viscosity and density measurements, The SVM 3000 viscometer was used, as shown in figure 4-8. A viscometer device measures the viscosity and density of crude oil, nanofluids, and alkali solutions. As a principle for measuring with this device, the viscometer automatically calculates the viscosity and density of the fluid sample. It delivered measurement results equivalent to ISO 3104 and was used for further calculations such as input to the IFT device.

Accuracy of the data collected is the primary concern for each measurement. In addition to the device's accurate calibration, the test was performed three times with average and standard deviation evaluations for each solution.

To ensure proper device calibration, the SVM 3000 Stainer viscometer can measure up to 30 samples at one time. Each sample has a different density and viscosity. Therefore, the viscometer has two solvents to clean the device automatically after finishing each measured sample. Otherwise, the measured data will not be accurate and has error values. After measured all samples, the data of all samples that include density and viscosity values were shown in the tables in chapter 5.

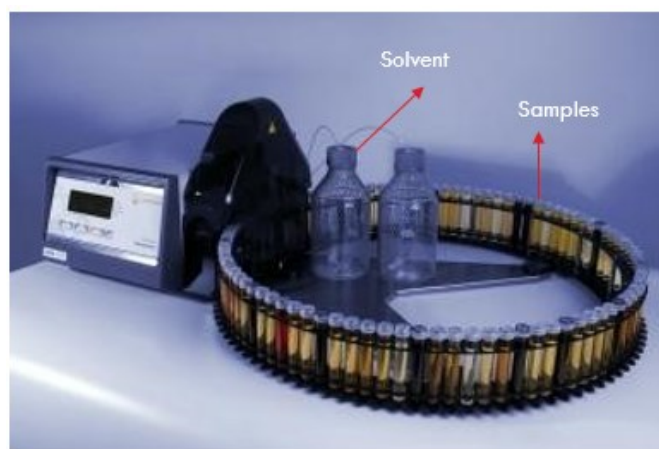


Figure 4-8 The SVM 3000 Stainer Viscometer (Armgate, 2015)

## 4.5 IFT Measurement

The IFT between the aqueous phase and the oil phase was measured with the help of a KRUSS spinning drop tensiometer, as shown in figure 4-9. The heavy fluid in this experiment includes the real and softened brine, and nanofluids at different concentrations, while the lighter fluid is crude oil.

The IFT was measured based on a compatibility screening test. The sample that contains precipitation was not considered. Consequently, the IFT was measured for samples that have

not any precipitation. The sample is placed in the vessel using a piston and a rod. Through the use of an auxiliary device, a droplet of oil is filled into the oil holder, and the oil holder is fixed into a vessel. Subsequently, the rod is removed, and the vessel can be placed inside the device. In this experiment, 19 types of IFT samples were measured at reservoir temperature conditions 73°C and 7000 rpm based on the principle suggested (Sharma et al., 1984).

The interfacial tension was calculated twice for each solution to determine the range of uncertainty. The IFT test results were observed and recorded over 150 minutes, revealing both instant IFT values equilibrium period of the IFT that expected to be established after the reaction between fluids and right after the experiment starts. The IFT was calculated using either the Young-Laplace model or the Vonnegut method based on the shape of the oil droplet

Furthermore, standard errors observed during the experiments could be related to various algorithms considered for the measurement based on the drop shape and fluid properties. Therefore, two separate algorithms for the measurements (Vonnegut and Young-Laplace) were considered to explain better and adequately depict the obtained data. The Vonnegut algorithm could not be extended for systems with interfacial tension more significant than 1 mN/m (Softened and real brine) due to the oil droplet's shape. As per the description, to use Vonnegut's method, the ratio between the oil droplet's length and width should be 4:1. For this reason, the measurement algorithm Young-Laplace has been used.

Meanwhile, the Young-Laplace process could not be used for systems with IFT lower than 1 mN /m (Nanofluids) due to the strongly elongated oil droplet. For this reason, the Vonnegut method was implemented. Each sample was measured two times to evaluate the accuracy of the method:



*Figure 4-9 A KRÜSS spinning drop tensiometer (Krüss scientific, 2018)*



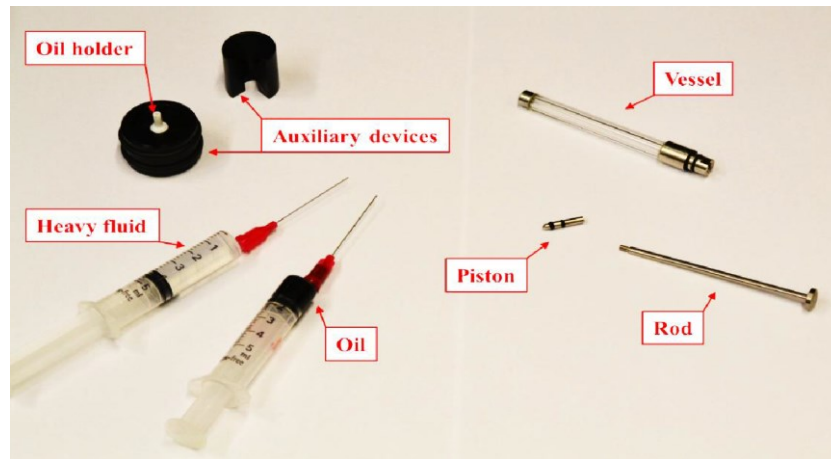


Figure 4-10 IFT-measuring device components (Arekhov 2019).



# Chapter 5

## Results and Discussion

This section discusses the results obtained during the different series of tests. It includes fluid analysis tests such as compatibility tests, phase behavior, dynamic viscosity, density, and IFT measurement.

### 5.1 Fluid Characterization Results

The viscometer device measured the crude oil and two synthetic brine real and softened. Table 5-1 and 5-2 below show the dynamic viscosity results and density of oil and real and softened brine at room temperature (25°C) and reservoir temperature (73°C).

*Table 5-1 Crude oil properties*

	<b>Dynamic viscosity, (mPs.s)</b>				<b>Density, (g/cm<sup>3</sup>)</b>			
	<b>25C°</b>		<b>73C°</b>		<b>25C°</b>		<b>73C°</b>	
	Mean	SD	Mean	SD	Mean	SD	Mean	SD
<b>OMV Crude Oil</b>	5,481	0,0337	1,8706	0,0434	0,8292	0,0005	0,7963	0,003

*Table 5-2 Synthetic brine properties*

<b>Parameter</b>	<b>Units</b>	<b>Real Brine</b>		<b>Softened Brine</b>	
		<b>Mean</b>	<b>SD</b>	<b>Mean</b>	<b>SD</b>
<b>Density, 25 °C</b>	<b>g/cm<sup>3</sup></b>	1,0397	0,0133	1,0408	0,0006
<b>Density, 73°C</b>		1,0275	0,0030	1,0128	0,0122
<b>Viscosity, 25°C</b>	<b>mPa.s</b>	1,1551	0,0982	1,1412	0,1276
<b>Viscosity, 73°C</b>		0,5850	0,1412	0,5028	0,0203

Furthermore, regarding types of nanofluids and alkali solution are present in appendix A.1

## 5.2 Compatibility Test

Two synthetic brine were prepared to investigate the effect of brine composition on the compatibility test. The compatibility test was performed with different types of nanofluids, namely S1, R1, P100, E100, A1, and A2 at different concentrations as shown in table 4-4, as well as alkali solution at 10 and 20 g/l for real brine and 1000 to 10000 ppm for softened brine. The real and softened brine were mixed with nanofluids and alkali solutions. All samples were put together in the oven at reservoir temperature, 73°C for 24 hours and one week to observe the compatibility fluid.

### 5.2.1 Nanofluid S1

#### 1. Compatibility Fluids at Time 0

It can be observed that there was no precipitation when nanofluid S1 was added to real brine at room temperature at different concentrations 10 wt%, 15wt%, 20 wt%, 25 wt%, and 30 wt%, as shown in figure 5-1. Therefore, the possible reason for surface modification of nanoparticles is that it stabilizes nanoparticles and prevents nanoparticles' aggregation in solution even in high salinity.

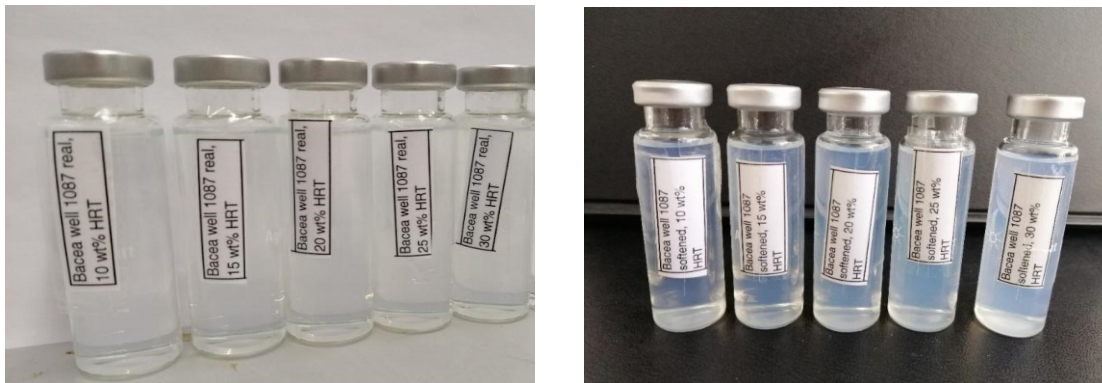


Figure 5-1 Nanofluid S1 at 10 wt%, 15wt%, 20 wt%, 25 wt%, 30 wt% (Left Real) (Right Softened) at (time 0)

In terms of nanofluids S1 in softened brine, it can be observed that nanofluid (S1) at a different concentration between 10 and 30 wt% did not have any precipitation, as shown in figure 5-1. The possible explanation is that softened brine as follow:

- a) Softened brine has a very low concentration of divalent cations  $\text{Ca}^{+2}$  and without  $\text{Mg}^{+2}$ , where divalent cations play a significant role in destabilizing particles (Wang & Alvarado, 2008).

- b) Surface modification of nanoparticles can also be that made stabilize nanoparticles and prevent aggregation nanoparticles in solution.

## 2. Compatibility Fluids at Time 24hr

It was clear to see from figure 5-2 that nanofluid S1 at 10,15,20,25 and 30 wt% in real brine has precipitation due to high temperature and salinity after 24 hours of observation. High temperature plays a significant role in destabilizing silica nanoparticles, causing aggregation of the nanoparticle and reducing electrostatic repulsions between the particles. Metin et al. (2011) reported the effect of temperature on the salinity in nanoparticles' presence. They found an increase in the average kinetic energy with temperature results in particle collisions, leading to aggregation. Therefore, a higher energy barrier, e.g., low salinity concentration, is necessary to maintain nanoparticle dispersion stability (Metin et al., 2011). For this reason, nanofluid S1 has precipitation after 24 hours in contrast to previous samples at 25°C that had no precipitation, as shown in figure 5-1. Also, The increased concentrations of nanofluids S1, the increase in precipitation.



*Figure 5-2 Nanofluid S1 at 10 wt%, 15wt%, 20 wt%, 25 wt% , 30 wt% (Left Real) (Right Softened) (after 24 hr)*

While Nanofluid (S1) softened, brine had no visible change even though they were exposed under high temperature 73°C, as shown in figure 5-2. The reason is in softened brine has not divalent cations that cause destabilizing particles and lead to aggregation.

## 3. Compatibility Fluids at Time one week

After one week, it can be observed that Nanofluid S1 real and softened have the same result as shown in figures 5-2.

**To sum up**, nanofluid S1 in softened brine did not show any visible change even though samples were exposed under high temperature, which is 73°C, which might be due to surface modification of nanoparticles that make stabilize nanoparticles and prevent aggregation

nanoparticles in solution. On the other hand, nanofluid S1 in real brine showed that have precipitation after exposed samples of nanofluids S1 at different concentrations at high temperatures. The reason is an increase in temperature from 25°C to 73°C, which leads to increases in the aggregation rate and divalent cations  $Mg^{+2}$  and  $Ca^{+2}$ , also effective in destabilizing nanoparticles and cause aggregation. Metin et al. (2011) reported a similar result.

Table 5-3 The observation of compatibility nanofluid S1

Nanofluid S1	Observation	
	Real Brine	Softened Brine
Time at 0	No visible change	No visible change
Time at 24 hr.	Precipitation	No visible change
Time at one week	Precipitation	No visible change

## 5.2.2 Nanofluid R1

### 1. Compatibility Fluids at Time 0

The results in nanofluid R1 at concentrations 1 and 2 gpt in real brine at room temperature, which is 25°C, did not show any precipitation, as shown in figure 5-3. Even though real brine has a high concentration of divalent cation such as  $Ca^{+2}$  and  $Mg^{+2}$ , the surfactants in nanofluid R1 can stabilize NPs in solution. Hence nanofluid R1 in real brine has not any precipitation.



Figure 5-3 Nanofluid R1 at 1 & 2 gpt (Left Real) (Right Softened) at (time 0)

In figure 5-2 (Right softened), it was observed that there was no visible change in nanofluid (R1) with softened brine at concentrations 1 and 2 gpt. This is because softened brine contains a very low concentration of divalent cations  $Ca^{+2}$ , and surfactant that present in nanofluid R1 played a vital role in stabilising NPs in solution nanofluid R1 in real brine has not any

precipitation. Zhao et al. (2018) reported a similar result influence on nanofluid stability, where surfactant adds to silica nanoparticle, and they observed that nanofluid is more stable.

**2. Compatibility Fluids at Time 24hr**

As for nanofluids (R1) at 1 and 2 gpt with real brine, there was a slightly cloudy like gel, as shown in figure 5-4. There are two possible explanations which are salinity and high temperature. The difference between nanofluid R1 at time 0 and time 24 hr is due to an increase in temperature from 25°C to 73°C, leading to increases in the aggregation rate and divalent cations  $Mg^{+2}$  and  $Ca^{+2}$  also effective in destabilizing nanoparticle and cause aggregation. On the other hand, Figure 5-4 (Right softened) shows that nanofluid (R1) in softened brine at 1, and 2 gpt has no precipitation.

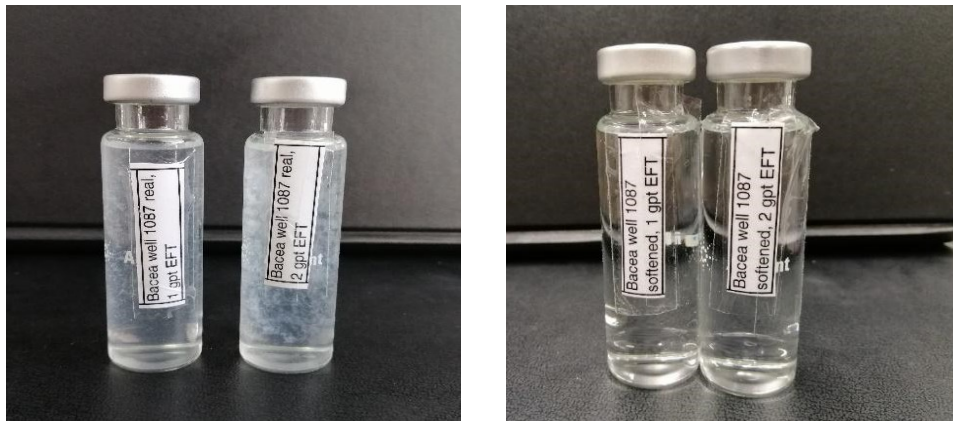


Figure 5-4 Nanofluid R1 at 1 & 2 gpt (Left Real) (Right Softened) (after 24 hrs.)

**3. Compatibility Fluids at Time one week**

After one week, it can be observed that Nanofluid R1 real and softened have the same result as shown in figures 5-4.

Table 5-4 The observation of compatibility nanofluid R1

Nanofluid R1	Observation	
	Real Brine	Softened Brine
Time at 0	No visible change	No visible change
Time at 24 hr.	Slightly cloudy like gel	No visible change
Time at one week	Slightly cloudy like gel	No visible change

### 5.2.3 Nanofluid E100 and P100

#### 1. Compatibility Fluids at Time 0

Nanofluids P100 and E100 at a concentration of 0.1 wt%, the results showed no precipitation when mixed with real brine, as shown in figure 5-13.



Figure 5-5 Nanofluid P100& E100 at 0.1 wt% (Left Real) (Right Softened) at (time 0)

As for softened brine with nanofluids E100 and P100 at concentration 0.1 wt%, it can be seen in figure 5-5 that there is not any precipitation. The possible reason is that softened brine has less concentration of divalent cation of  $\text{Ca}^{+2}$  because divalent cation  $\text{Ca}^{+2}$  and  $\text{Mg}^{+2}$  are more effective in destabilizing particles. Therefore, nanoparticles will be stable and electrostatic repulsions between the particles is high (Metin et al., 2011).

#### 2. Compatibility Fluids at Time 24 hr

Figure 5-6 illustrates that nanofluids P100 and E100 for real has low precipitation. While nanofluid P100 has low precipitation with softened brine. In contrast, nanofluid E100 showed there was no visible change.

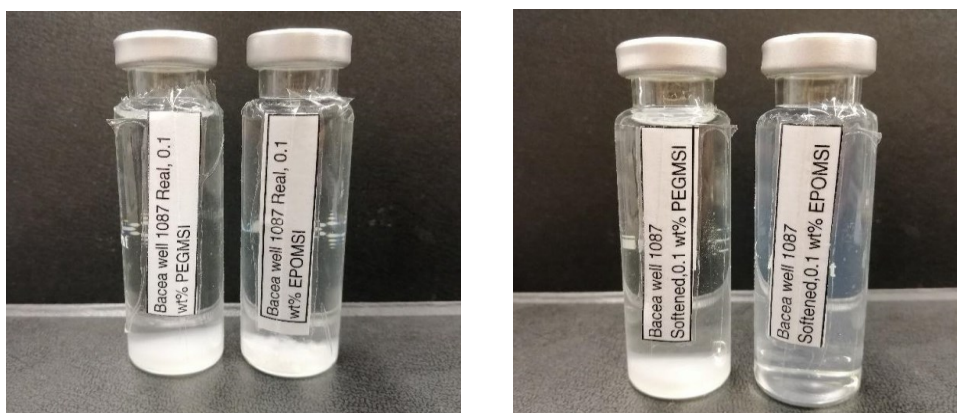


Figure 5-6 Nanofluid P100& E100 Real at 0.1 wt% (Left Real) (Right Softened) (after 24 hrs.).



### 3. Compatibility Fluids at Time one week

After one week, it can be observed that Nanofluids E100 and P100real and softened have the same result as shown in figures 5-6.

**To sum up**, even though nanofluids P100 and E100 have the same type and almost the same size and dimensions, P100 has precipitation in contrast E100. This reason due to different surface charges in nanofluid P100 that was neutral charge ranging from -3 to -8 mV while nanofluid E100 was a negative charge (-14 to -18mV) and hence the addition of salt in solution and high temperature which in result change the zeta potential to zero and cause aggregation of NPs. Moreover, Yu & Xie (2012) reported that the zeta potential, either positive or negative at a low value around zero, tends to coagulate or flocculate, but at high zeta potential has excellent stability. While nanofluid of P100 has reacted by softened brine and has precipitation. On the contrary, nanofluid softened of E100 has not reacted by softened brine, and there is no precipitation, as shown in figure 5-6.

*Table 5-5 The observation of compatibility nanofluids E100 & P100*

Observation				
	Nanofluid E100		Nanofluid P100	
	Real Brine	Softened Brine	Real Brine	Softened Brine
Time at 0	No visible change	No visible change	No visible change	No visible change
Time at 24 hr.	Precipitation	No visible change	Precipitation	Precipitation
Time at one week	Precipitation	No visible change	Precipitation	Precipitation

## 5.2.4 Nanofluid A1 and A2

### 1. Compatibility Fluids at Time 0

Figures 5-7 and 5-8 show that nanofluid A1 at concentrations 10 and 20 wt% has no reaction or precipitation with softened brine. In contrast, it was noticed that nanofluid A2 at concentrations 10 and 20 wt% there was a slightly cloudy gel in softened brine.

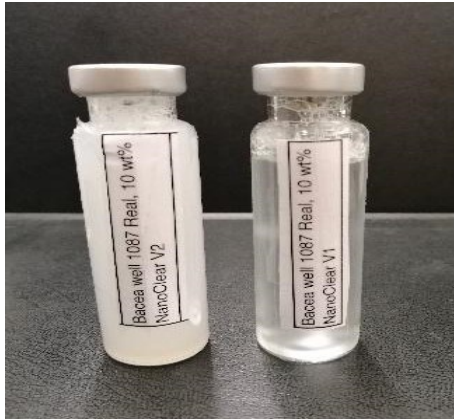


Figure 5-7 Nanofluids A1 & A2 at 10 wt% (Left Real) (Right Softened) at (time 0)

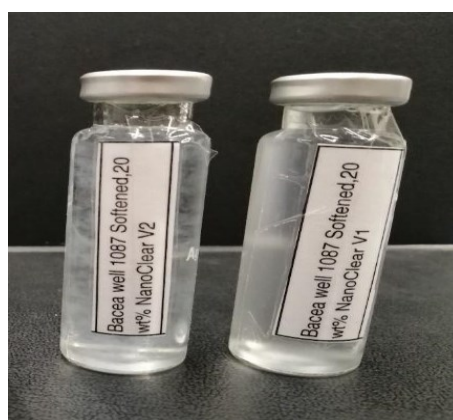
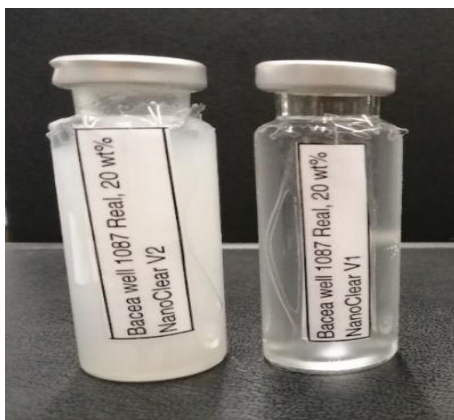


Figure 5-8 Nanofluids A1 & A2 at 20 wt% (Left Real) (Right Softened) at (time 0)

## 2. Compatibility Fluids Real at Time 24 hr

In terms of nanofluid A1 and A2 real, it can be seen that nanofluid A1 at concentrations 10 and 20 wt% have no visible change. In comparison, nanofluid A2, there was precipitation and agglomeration at concentrations 10 and 20 wt%, as shown in figures 5-9 and 5-10.

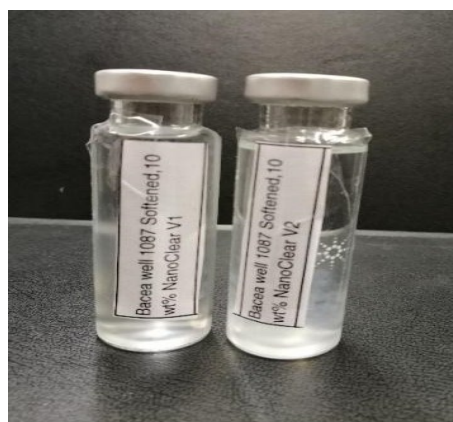
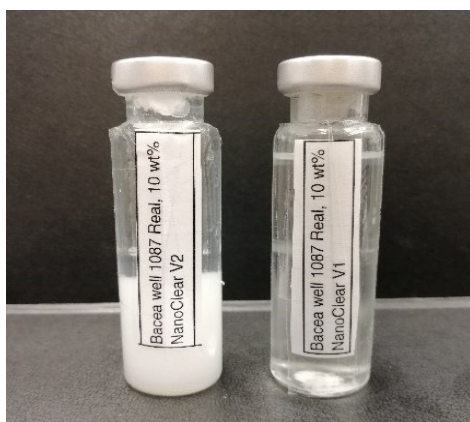


Figure 5-9 Nanofluids A1 & A2 (Left Real) (Right Softened) at 10 wt% (after 24 hrs.).

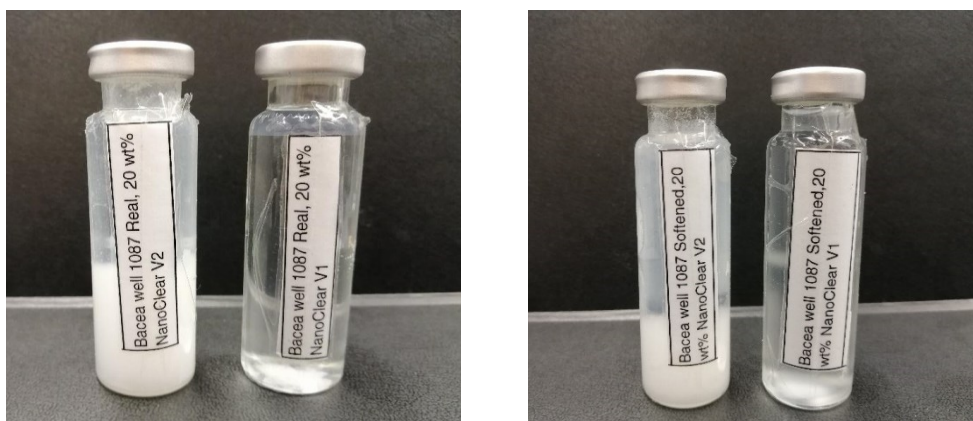


Figure 5-10 Nanofluids A1 & A2 ( (Left Real) (Right Softened) at 20 wt% (after 24 hrs.).

The nanofluid A2 for softened at 10 wt% has reacted with softened brine and has gel in the solution, while nanofluid A1 has no visible change, as shown in figure 5-9. Also, the second concentration of 20 wt% for nanofluids A1 and A2 are similar results with 10 wt%.

The main reason behind precipitation in nanofluid A2 could be two possible explanations: the divalent cation of  $Ca^{+2}$  and  $Mg^{+2}$  presence in real brine, which reduces electrostatic repulsions between the particles (Metin et al., 2011). Also, it could be due to salts in solution change the value of zeta potential to zero, which leads to aggregation of NPs in the solution, where zeta potential is directly related to the surface charge of the NPs in solution (Olayiwola & Dejam, 2019).

### 3. Compatibility Fluids at Time one week

After one week, it can be observed that nanofluid A1 and A2 real and softened at concentrations 10 and 20 wt% have the same result as shown in figures 5-9 and 5-10.

Table 5-6 The observation of compatibility nanofluids A1 & A2

Observation				
	Nanofluid A1		Nanofluid A2	
	Real Brine	Softened Brine	Real Brine	Softened Brine
Time at 0	No visible change	No visible change	Precipitation	Slightly cloudy like gel
Time at 24 hr.	No visible change	No visible change	Precipitation	Slightly cloudy like gel
Time at one week	No visible change	No visible change	Precipitation	Precipitation

## 5.2.5 Alkaline solution $\text{Na}_2\text{CO}_3$

### 1. Compatibility Fluids Real at Time 0

Sodium carbonate ( $\text{Na}_2\text{CO}_3$ ) triggers precipitation due to the presence of divalent cations  $\text{Ca}^{+2}$  and  $\text{Mg}^{+2}$  in real brine. Calcium ( $\text{Ca}^{+2}$ ) reacts with carbonate ( $\text{CO}_3^{-2}$ ), which causes precipitation, as shown in figure 5-11. Therefore, alkali is not recommended when brine formation is rich with divalent cations (Spanos & Koutsoukos, 1998).

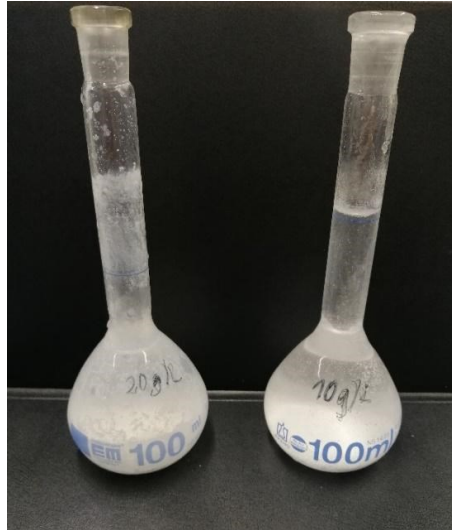


Figure 5-11 Alkaline solution (Real brine) at 10 & 20 g/l

### 2. Compatibility Fluids Softened at Time 0

Moreover, alkali solutions ( $\text{Na}_2\text{CO}_3$ ) at a concentration (1000-10000 ppm) have no visible change due to that softened brine has a low concentration of divalent cation of  $\text{Ca}^{+2}$ . For this reason,  $\text{Na}_2\text{CO}_3$  could not react with the divalent cation of  $\text{Ca}^{+2}$  as shown in Figures 5-12.



Figure 5-12 Alkaline ( $\text{Na}_2\text{CO}_3$ ) Softened brine at (1000-10000 ppm) at (time 0).

Table 5-7 The observation of compatibility alkali solution

Alkaline (Na <sub>2</sub> CO <sub>3</sub> )	Observation	
	Real Brine	Softened Brine
Time at 0	Immediate floc formation	No visible change
Time at 24 hr.	Precipitation	No visible change
Time at one week	Precipitation	No visible change

Figures 5-13 and 5-14 indicates all nanofluids at the different concentration for real and softened brine after one week of observation at reservoir temperature.

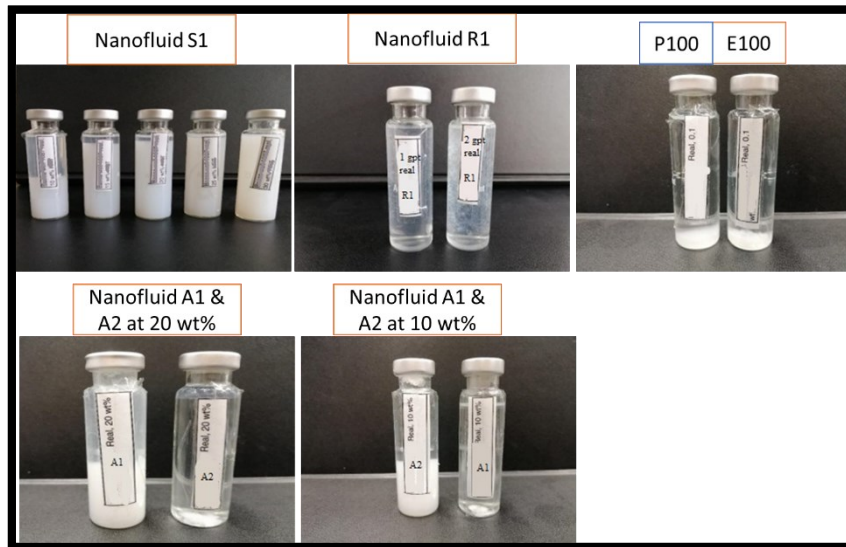


Figure 5-13 All nanofluids for real brine after one week of observation

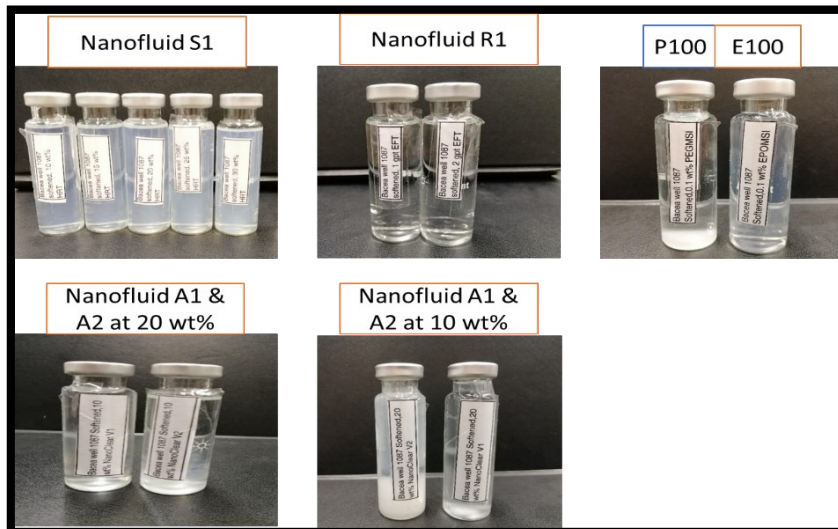


Figure 5-14 All nanofluids for softened brine after one week of observation

Table 5-8 The summary of nanofluids for real and softened brine

Samples	Real Brine			Softened Brine		
	Time 0 at 25 °C	After 24 hours at 73°C	One week at 73°C	Time 0 at 25 °C	After 24 hours at 73°C	One week at 73°C
Nanofluid S1	No visible change	Precipitation	Precipitation	No visible change	No visible change	No visible change
Nanofluid R1	No visible change	Slightly cloudy like gel	Slightly cloudy like gel	No visible change	No visible change	No visible change
Nanofluid E100	No visible change	No visible change	Precipitation	No visible change	No visible change	No visible change
Nanofluid P100	No visible change	Precipitation	Precipitation	No visible change	Precipitation	Precipitation
Nanofluid A1	No visible change	No visible change	No visible change	No visible change	No visible change	No visible change
Nanofluid A2	Precipitation	Precipitation	Precipitation	Slightly cloudy like gel	Slightly cloudy like gel	Precipitation

### 5.3 Phase Screening Evaluations

The main aim of phase behavior experiments is to study the emulsification process and the emulsion's stability by monitoring the position of the interface between oil, water, and emulsion phase over time. The type of nanomaterial surface modification had a negligible effect on the stabilized emulsion volume.

#### 5.3.1 Influence of nanofluids on emulsion formation with real brine

##### Nanofluid S1

In the experiment, nanofluid S1 real at concentrations 10, 15, 20, 25, and 30 wt%, the concentration 20, 25, and 30 wt% of nanofluid S1 have a high initial emulsion volume was observed directly after mixing as shown in figure 5-13. In comparison, nanofluid S1 at concentrations 10 and 15 wt%, there is no emulsion in the above image. The increase in the concentration of nanofluid S1 results in a rise in the initial emulsion volume. Besides, it can be observed that type of phase behavior is seen as Winsor (type II) water in oil emulsion. This result correlates to the literature where those are mentioned for high salinity brines. Note that,

it was difficult to determine whether there was an emulsion phase, particularly within the first week of the experiment.



Figure 5-15 Phase experiments (after mixing) with 10, 15, 20, 25 & 30 wt% of (S1).

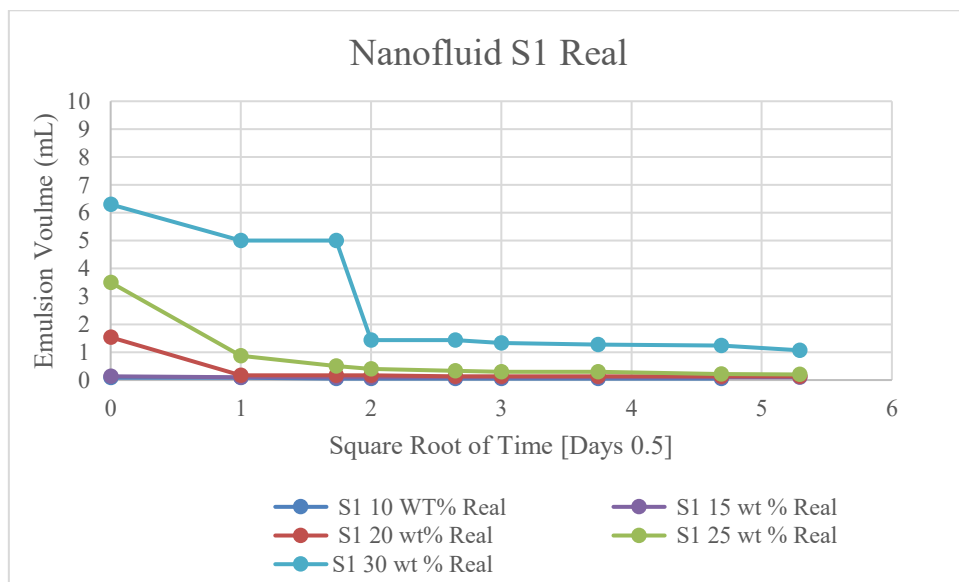


Figure 5-16 Emulsion volume over 30 days and 73 °C with crude oil and nanofluid S1 Real at different concentrations.

The observations obtained for nanofluids at different concentrations for 30 days (as shown in Figure 5-16) can be summarized as follow:

1. For the experiment with nanofluid (S1) at concentration 10 wt%, nanofluid S1 had a low emulsion volume with 0.1 mL on the first day, and then still stable at 0.05 mL for 30 days.
2. For nanofluid S1 at 15 wt%, the initial emulsion volume was low with 0.15 mL, and then it was stable at 0.1 mL for more than 30 days.
3. In the presence of nanofluid S1 at 20 wt%, the initial emulsion volume was again low (approximately 2 mL). The emulsion volume was constant at ~0.05 mL until the end of the investigation.
4. As for nanofluid S1 at 25%, %, the initial emulsion volume was almost 3.5 mL. After five days, the emulsion volume was decreasing until it reached ~0.05 mL
5. The initial emulsion volume was high during experiments nanofluid S1 at 30 wt% (approximately 6.3 mL). After 30 days, however, the emulsion volume was low and stable at 1 mL.

### **Discussion**

The increasing concentration of nanofluid S1 will have several particles that lead to accumulating or adsorbed at the interface between the oil and aqueous phase and will have an emulsion (Wang & Alvarado, 2008). After a few days, samples were exposed under 73°C that it can be observed particles has precipitation due to high temperature and high salinity, and hence emulsion volume starts to decrease due to particles were destabilized at the interface between oil and aqueous phase. Two possible explanation for reducing emulsion behavior:

- a) The brine phase's salinity, is the concentration of divalent cations  $\text{Ca}^{+2}$  and  $\text{Mg}^{+2}$  that plays an essential role in emulsions' stability (Wang & Alvarado, 2008). Besides, particles tend to be more flocculated due to the reduction in electrostatic repulsions between the particles. As a result, particles will decrease their sorption at the oil-water interface (McElfresh et al., 2012).
- b) The composition of the oleic phase includes asphaltene content, where asphaltene are precipitated which causes loss of emulsion stability (Grutters et al., 2007).

Furthermore, a brownish coloring and high turbidity of the aqueous phase might be pointing out a loss of additional NSO-compounds or lost aliphatic and aromatic compounds in the water phase (Leitenmüller & Rupprecht, 2019). Unfortunately, the concentration of the hydrocarbon content in the aqueous phase had not been possible reliably measured. A similar result was reported for NPs with high TAN oil by (Neubauer et al., 2020 b). They found brownish color in the aqueous phase at different concentrations of nanoparticles.



### Nanofluid R1

Results obtained from experiment nanofluid R1 at concentrations 1 & 2 gpt indicated after mixing samples that there was no emulsion between the oil phase and aqueous phase, as shown in Figures 5-17. Also, the samples were set in the oven at 73°C for 30 days and showed no visible change. There is two possible explanation for reducing emulsion behavior:

- The concentration of surfactant in nanofluid R1 is not enough to create and react with crude oil due to the crude oil has low TAN, which is (0.13 mg KOH/g) (Sheng, 2015).
- The salinity in real brine was high, which cause destabilized nanoparticles and reduce electrostatic repulsions between the particles. As a result, particles will decrease their sorption at the oil-water interface, and hence emulsion stability decreases (McElfresh et al., 2012).



*Figure 5-17 Phase experiments with 1 & 2 gpt of nanofluid R1*

### Nanofluid A1 and A2

It can be observed from Figures 5-18 and 5-19 that nanofluids A1 and A2 at 10 & 20 wt% showed a high initial emulsion volume after mixing samples, where this is visible by the eye but does not show in the pictures. The type of phase behavior is seen to be Winsor (type I) oil in water emulsion. Note that it was difficult to determine whether there was an emulsion phase, particularly within the first week of the experiment.



Figure 5-18 Phase experiments with nanofluids A1 & A2 at 10 wt%,

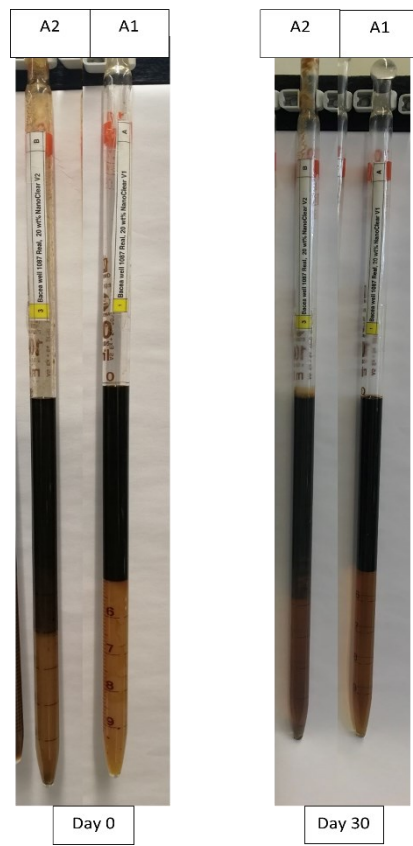


Figure 5-19 Phase experiments with nanofluid A1 & A2 at 20 wt%,.

The observation obtained from nanofluid A1 & A2 real at concentration 10 and 20 wt% as shown in figures 5-18 and 5-19 can be summarized as follow:

1. The experiment of nanofluid A1 for real at 10 wt% showed a high initial emulsion volume which is 5 mL. After 30 days, the emulsion volume was still stable at 0.1 wt%. The type of phase behavior is Winsor (type I) which means oil in water phase emulsion.
2. The experiment with nanofluid A1 at 20 wt% illustrated that the initial emulsion volume was 5 mL. After a few days, the emulsion volume declined to 0.05 mL, where the type of emulsion is Winsor (type I) oil in water phase emulsion.
3. For the experiment with nanofluid A2 at 10 wt% for real, it can be observed that the initial emulsion volume was 5 mL, and after four days, the emulsion volume was still stable at 0.05 mL. The type of emulsion is Winsor (type I) oil in water phase emulsion.
4. In the presence of A2 at 20 wt%, it can observe that there was a high initial emulsion which is around 6 mL, and the type of phase behavior is Winsor (type I) which means that oil in water phase emulsion, as shown in figure 5.42.

### Discussion

1. The concentration of nanofluid A2 at 20 wt% was higher than nanofluid A2 at a concentration of 10 wt% in terms of initial emulsion volume, as shown in figures 5-18 and 5-19. The possible explanation is that nanoparticles are a stronger tendency to adsorb and accumulate at the interfaces. Also, an increase in nanofluids' concentration led to an increase in the number of particles and adsorbed and create emulsion volume (Arab et al., 2018).
2. After few days, the emulsion volume was very low, which might be due to high temperature and divalent cation  $\text{Ca}^{+2}$  and  $\text{Mg}^{+2}$  that causes to prevent the accumulation of particles at the interface between oil and aqueous phase. Hence, nanoparticles will be precipitated (Wang & Alvarado, 2008). Some researchers,  $\text{Mg}^{+2}$  is the most effective in destabilizing nanoparticles and emulsion (Tambe and Sharma, 1993). In terms of nanofluid A1 at different concentrations, 10 and 20 wt% showed no emulsion, as shown in figures 5-18 and 5-19.
2. The brownish color and high turbidity of the aqueous phase might have been attributed to aliphatic and aromatic compounds, as shown in figures 5-18 and 5-19 (Leitenmüller & Rupprecht, 2019). Neubauer et al., (2020 b) reported a similar result for nanomaterial at different concentrations with high TAN oil. The result showed a brownish color in an aqueous phase, where it was difficult to know if this brownish color is an emulsion at the first week.

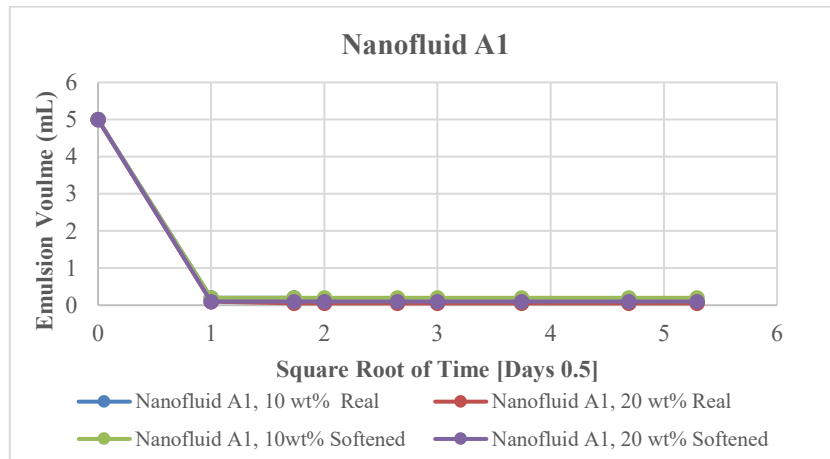


Figure 5-20 Emulsion volume over 30 days and 73 °C for nanofluid A1 Real & Softened at 10 & 20 wt%.

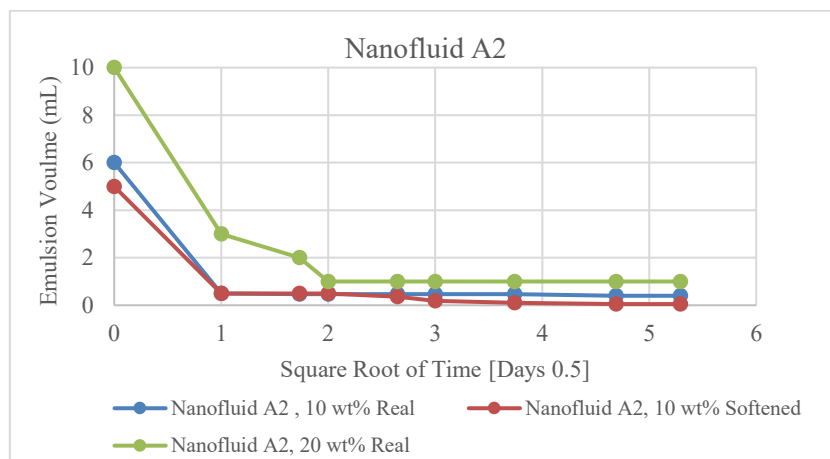


Figure 5-21 Emulsion volume over 30 days and 73 °C for nanofluid A2 Real & Softened at 10 & 20 wt%

### Nanofluid E100 and P100

The result obtained from experiment nanofluids E100 and P100 at concentration 0.1 wt% showed no emulsion, as shown in figure 5-22. The samples of both nanofluids E100 and P100 were set in the oven at 73°C for 30 days, and results showed no visible change. The possible explanation for emulsion behavior; the salinity in real brine was high, which cause destabilized nanoparticles and reduce electrostatic repulsions between the particles (Metin et al., 2011). As a result, particles will decrease their sorption at the oil-water interface, and hence there will not be any reaction with oil, which means no emulsion.

Results obtained in this experiment show a similar behavior as those reported by (Neubauer et al., 2020 b) for select nanofluids as emulsion stabilizers. They found that nanoparticles could not create an emulsion.



Figure 5-22 Phase experiments with 0.1 wt% of P100 & E100.

### 5.3.2 Influence of Nanofluids on Emulsion Formation for Softened Brine

#### Nanofluid S1

The concentration of nanofluid S1 softened at 10, 15, 20, 25, and 30 wt% have a high initial emulsion volume that was observed directly after mixing for 64 hours as shown in figure 5-23.



Figure 5-23 Phase experiments with 10, 15, 20, 25 & 30 wt% of (S1) Softened

The increase in the concentration of nanofluid S1 increases the initial emulsion volume (Tambe and Sharma, 1993). Besides, it can be observed that type of phase behavior is seen as Winsor (type II) water in oil emulsion. This result correlates to the literature where those are mentioned for high salinity brines.

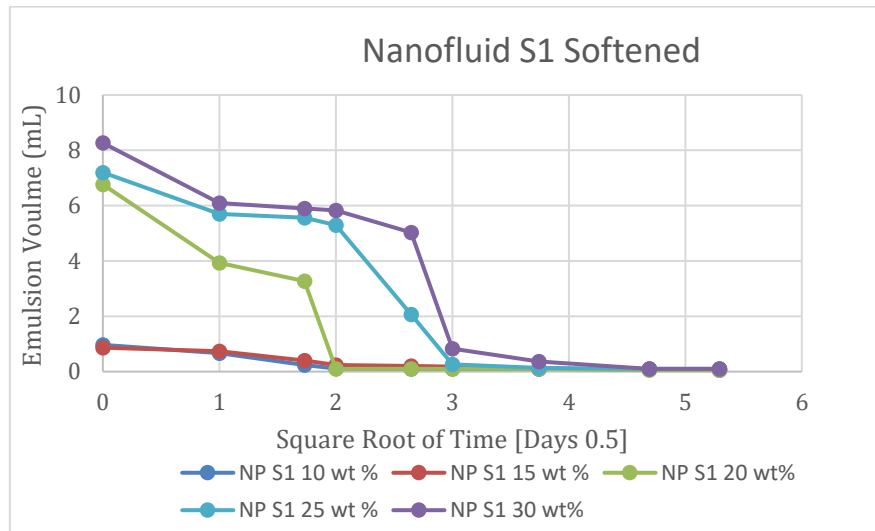


Figure 5-24 Emulsion volume over 30 days and 73°C for (S1) Softened at different concentrations

Observations obtained for nanofluid (S1) Softened at different concentrations 10, 15, 20, 25, and 30 wt%, as shown in figure 5-24, can be summarized as follow:

1. In an experiment of nanofluids (S1) 10 wt%, the initial emulsion volume was low, and after two days, the emulsion volume was constant at 0.05 mL.
2. In the presence of nanofluid (S1) 15 wt%, the initial emulsion volume had an almost equal volume to concentration nanofluid (S1) 10 wt%, which is about 1.2 mL. After that, the emulsion volume decreasing steadily to 0.05 mL.
3. The initial emulsion volume was high during the experiment with nanofluid (S1) 20 wt%, resulting in approximately 7 mL before the drop to 0.05 mL.
4. For (S1) 25 wt%, the initial emulsion volume was again high for experiments. However, after nine days, the emulsion volume decreased to 0.05 mL, and it remained constant until the end of the investigation.
5. At nanofluid (S1) 30 wt%, the initial emulsion volume was again high, which is more than 8 mL, and then decreasing slightly for 9 days, reaching 0.05 mL. The emulsion volume was constant at ~0.05 mL until the end of the investigation.

## Discussion

1. The increased concentration of nanofluid S1 softened lead to increase emulsion volume after pipette shaking. The possible explanation is that nanoparticle accumulates or absorbed at interface oil and aqueous phase to create an emulsion.
2. After few days, it can be observed that emulsion volume was low because high salinity (NaCl) causes to prevent accumulate of particles at the interface between oil and the aqueous phase (Kim et al., 2016). Besides, In the emulsion process, the agglomeration of the nanoparticles can create a rigid layer of emulsion droplets that may serve as a

coalescence barrier, and hence emulsion will be reduced. (McElfresh et al., 2012) reported similar results.

3. The nanofluid S1 in softened was a higher initial emulsion volume than nanofluid S1 in real. Softened brine has a low concentration of divalent cation  $\text{Ca}^{+2}$  and, without  $\text{Mg}^{+2}$ , is considered more effective in destabilizing nanoparticles. Therefore, nanofluid S1 softened has a more stable nanoparticle. A similar result was reported by Tambe and Sharma (1993) that divalent cation and sodium chloride substantially affect emulsion stability and emulsion volume.

### Nanofluid R1

Results obtained from experiment nanofluid R1 in softened brine at concentrations 1 & 2 gpt indicated after mixing samples that there was no emulsion between the oil phase and aqueous phase, as shown in figure 5-25. Also, the samples were set in the oven at  $73^{\circ}\text{C}$  for 30 days and showed no visible change. Moreover, nanofluid R1 in real and softened showed the same result and reason.



Figure 5-25 Phase experiments with 1 & 2 gpt of nanofluid (R1)



### Nanofluid A1 and A2

It can be observed that the initial emulsion volume was high after mixing samples nanofluid A2 at 10 wt%, and the type of phase behavior is seen to be Winsor (type I) oil in water emulsion. While nanofluid A1 at 10 wt% showed, there was emulsion as shown in figure 5-26. Besides, Nanofluid A2 at concentration 20 wt% showed high initial emulsion volume, as shown in figure 5-27. Besides, nanofluid A1 at 20 wt% showed a high initial emulsion volume after pipettes were shaken.

The observation obtained from nanofluid A1 & A2 softened at concentration 10 and 20 wt% as shown in figures 5-18 and 5-19 can be summarized as follow:

1. The experiment of nanofluid A1 for real at 10 wt% showed a high initial emulsion volume which is 5 mL. After few days, the emulsion volume was still stable at 0.1 wt%.
2. The experiment with nanofluid A1 at 20 wt% illustrated that the initial emulsion volume was 5 mL, and after a few days, the emulsion volume decline to 0.05 mL.
3. For the experiment with nanofluid A2 at 10 wt% for real, it can be observed that the initial emulsion volume was 5 mL, and after four days, the emulsion volume was still stable at 0.05 mL.
4. In the presence of A2 at 20 wt%, it can observe that there was a high initial emulsion which is around 5 mL. After few days, the emulsion volume was still stable at 0.1 wt%. as shown in figure 5.27.



Figure 5-26 Phase experiments with Nanofluid A1 & A2 10 wt%



Figure 5-27 Phase experiments with nanofluid A1 & A2 20 wt%

**The results obtained from nanofluids A1 & A2 experiments can be analyzed as follow:**

1. The concentration of nanofluid A2 at 20 wt% was higher than nanofluid A2 at a concentration of 10 wt% in terms of initial emulsion volume. The main reason is that nanoparticles accumulate toward at interface between oil and the aqueous phase. Hence, the increase of concentration of nanofluids led to an increase in the number of particles and adsorbed and creates emulsion volume, as shown in figures 5-26 and 5-27. Note that nanofluid A2 has higher precipitation in the compatibility test, which means it is unsuitable for the emulsion phase.
2. After few days, it can be observed that emulsion volume was low due to high salinity that causes to prevent accumulate of particles at the interface between oil and aqueous phase, and hence nanoparticles will be precipitated. Moreover, In the emulsion process, the agglomeration of the nanoparticles can create a rigid layer of emulsion droplets that may serve as a coalescence barrier, and hence emulsion will be reduced (Kim et al., 2016).

### **Nanofluid E100 and P100**

The result obtained from experiment nanofluids E100 and P100 at concentration 0.1 wt% showed no emulsion, as shown in figure 5-28. Besides, the samples of both nanofluids E100 and P100 were set in the oven at 73°C for 30 days. As a result, samples showed no visible

change. Note that nanofluid E100 and P100 in real and softened brine have the same observed or result.

This experiment results reveal similar behavior as those reported by Neubauer et al. (2020) for select nanofluids as emulsion stabilizers. They found that nanoparticles could not create an emulsion.



Figure 5-28 Phase experiments with 0.1 wt% of nanofluid P100 & E100, Blue lines: oil/brine interface

### Sodium Carbonate $\text{Na}_2\text{CO}_3$

In an experiment alkali, sodium carbonate  $\text{Na}_2\text{CO}_3$  at different concentrations from 1000 to 10000 ppm. After the tube was shaken, it can be observed that there was no emulsification solely generated by sodium carbonate with low TAN crude oil despite the use of sodium carbonate solution different concentrations from 1000 to 10000 ppm as shown in figure 5-29. After setting all sodium carbonate solution samples at different concentrations in the oven at  $73^\circ\text{C}$  for 30 days. As a result, it can be seen that there was no visible change.

The possible explanation for this result is the total acid number of crude oil. The crude oil has a very low TAN (0.13 mg KOH/g), and hence sodium carbonate  $\text{Na}_2\text{CO}_3$  solution could not react with oil to generate emulsion at the oil/water interface. Also, it requires a sufficiently high concentration of  $\text{Na}_2\text{CO}_3$ . Sheng (2015) reported similar results for Alkalis to react with low TAN oil at low concentrations of divalent cation  $\text{Ca}^{+2}$ .



Figure 5-29 Phase experiments with Alkaline solution at (1000-10000) with 1000 step, Blue lines: oil/brine interface.

## 5.4 Interfacial Tension

In this experiment, 13 samples of IFT were measured using the spinning drop technique. Note that nanofluid samples were chosen based on the compatibility test with no precipitation either in real or softened brine. The behavior of the IFT reduction depends on the concentration, size, and type of nanoparticles. Real brine containing divalent cations  $\text{Ca}^{+2}$  and  $\text{Mg}^{+2}$  and softened brine without divalent cations substantially affects the IFT system's behavior.

### 5.4.1 The real & softened brine

#### Observation

The interfacial tension in the oil/real brine system stabilized at 10.85 mN/m after 100 minutes of observation (figure 5-30, blue dots), while IFT between crude oil and softened brine was  $\sim 7.14$  mN/m after 130 minutes of observation, as shown in figure 5-30 (red dots).

Results obtained indicate a difference between real and softener brine results, as shown in Figures 5-30 below. The real brine showed higher IFT with low TAN oil than softened brine by almost 3 mN/m.

## Discussion

The possible explanation for the different IFT behavior is that divalent cations  $\text{Ca}^{+2}$  and  $\text{Mg}^{+2}$  in brine have stronger effects on IFT in higher salinity, where real brine has a higher concentration of salinity  $\sim(84 \text{ g/l})$  with divalent cations  $\text{Ca}^{+2}$  and  $\text{Mg}^{+2}$ . On the contrary, softened brine has a lower concentration salinity  $\sim (65 \text{ g/l})$  without divalent cations than real brine.

Rostami et al. (2019) reported a similar result for high salinity systems, the presence of divalent  $\text{Ca}^{+2}$  and  $\text{Mg}^{+2}$  cations cause increase IFT, and hence the low concentration of  $\text{Ca}^{+2}$  leads to reduce IFT. Due to this consequence, the existence of divalent cations such as calcium and magnesium in high salinity systems can deplete the surface-active agent interface and thus lead to higher IFT. Furthermore, the increase in the ratio of cation charges ( $z^+$ ) to cation surface area ( $r^2$ ) plays a significant role in increasing the attraction of cations to the interface, and hence IFT increases (Divandari et al., 2020). Moreover, the increase in the salinity concentration in the aqueous phase increases the aqueous phase's density. Hence, it increases the density difference between the oil phase and aqueous phases, which increased IFT.

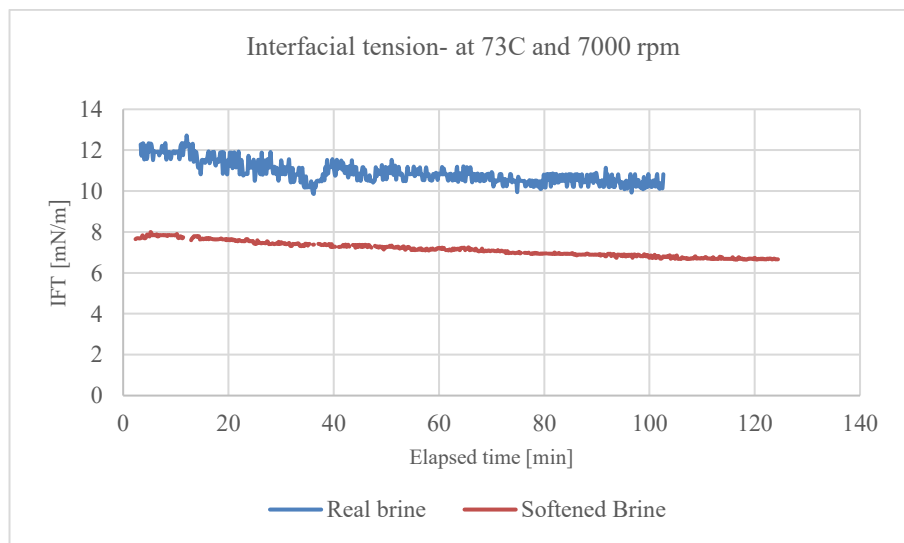


Figure 5-30 The IFT of real and softened brine

### 5.4.2 Nanofluids

Nanofluid has a significant ability to reduce IFT compared to the base case (real and softened brine). Due to nanoparticles that like surfactant molecules, could spontaneous adsorption of particles at the fluid-fluid interface or the nanoparticles accumulating in the interfacial layers (Huh et al., 2019).

## Observation

The IFT between nanofluid S1 softened, and crude oil was low, approximately between 0.43 and 0.53 mN/m after 150 minutes of observation, as shown in Figures 5-31. It can also observe from figures 5-30 and 5-31 that IFT reduced from 7.14 mN/m (crude oil and softened brine) to 0.43 and 0.53 mN/m when adding nanofluids S1 softened.

Nanofluid S1 in softened at concentration 10 wt% (figure 5-31, red dots) showed that it has the lowest IFT  $\sim 0.43$  mN/m compared to other concentrations. In general, the IFT between nanofluid S1 at different concentrations in softened water and crude oil illustrated no high difference between them in terms of IFT reduction values. Note that the light-colored areas are corresponding to standard deviation.

Moreover, figure 5-31 also illustrates the IFT between nanofluid R1 at concentrations 1 & 2 gpt and crude oil. The results showed that the IFT of nanofluid R1 in real brine has lower IFT than nanofluid R1 in softened brine at concentrations 1 and 2 gpt after 150 minutes of observation. Nanofluid R1 real at concentrations 1 and 2 gpt are close by values of IFT, which are 0.19 and 0.176 mN/m, respectively. The IFT between low TAN crude oil and nanofluid R1 softened at 1 gpt was  $\sim 0.35$  mN/m, while nanofluid R1 in softened at 2 gpt was  $\sim 0.46$  mN/m.

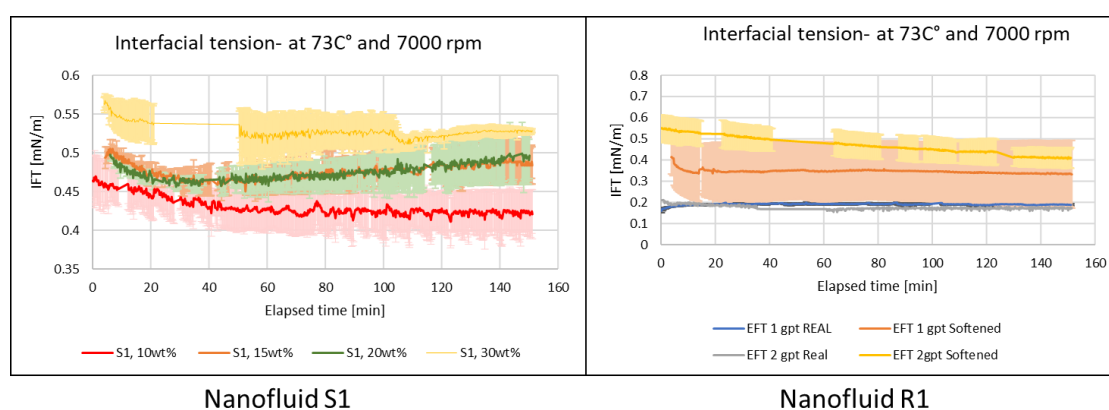


Figure 5-31 The IFT between nanofluid S1 (10 – 30 wt%) & nanofluid R1 and crude oil.

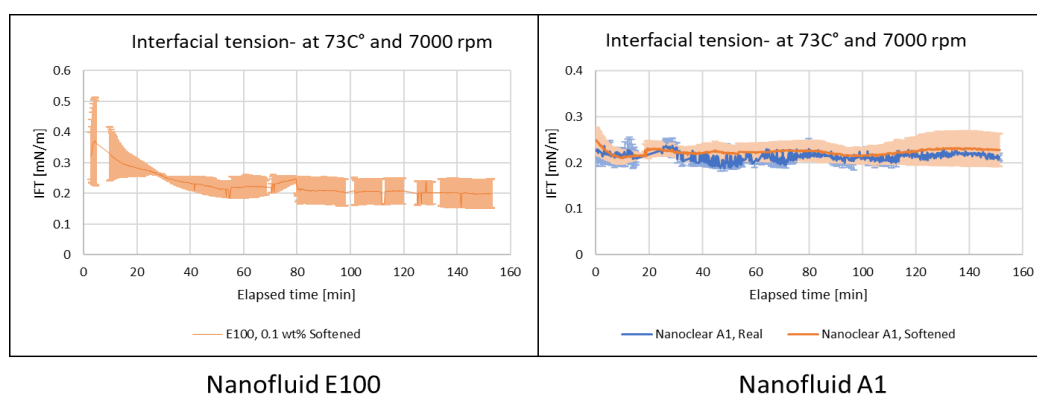


Figure 5-32 The IFT between nanofluid E100 & A1 and crude oil

In figure 5-32 the IFT between low TAN crude oil and nanofluid A1 in real and softened brine was observed after 150 minutes. The results illustrate that the values of IFT reduce in crude oil and real brine system from 10.85 mN/m to 0.215 mN/m after adding 0.1 wt% of nanoparticle A1 in real brine, while the IFT for between oil and nanofluid A1 in softened brine was almost 0.223 mN/m. Furthermore, the IFT between low TAN crude oil and nanofluid E100 at concentration 0.1 wt% softened brine was low  $\sim$  0.233 mN/m, as shown in figure 5-32.

## Discussion

**Nanofluid S1** real was not measured due to high precipitation. However, the results obtained from nanofluid S1 softened showed that it has low IFT at different concentrations (10,15,20,25, and 30 wt%) between 0.43 and 0.53 mN/m.

The main reason for the IFT reduction is the adsorption of surface-modified silicon dioxide NPs at the oil-water interface. Therefore, the size of NPs can play an essential role in effect IFT. The particle size decrease, the number of particles in the volume unite of nanofluid increases. Accordingly, a higher number of nanoparticles accumulate in the interfacial layers and reduce IFT. Neubauer et al. (2020) reported a similar result. A similar influence on IFT behavior for n hexane-water samples containing different sized silica nanoparticles was reported (Saïen & Bahrami, 2016).

Moreover, The different concentrations of nanofluids S1 showed no significant difference in terms of IFT reduction. Previous research showed that further increases in the concentration had no impact on the interfacial tension (Alnarabiji & Husein, 2020).

**Nanofluid R1**, it can be observed that nanofluid R1 for real has the lowest IFT, which is 0.17 mN/m compared to nanofluids A1 and E100 in softened brine, as shown in table 5-9. Nanofluid R1 contains a surfactant, solvent, and surface-modified silica particles, where surfactant enhances the stability of nanoparticles in solution and reduces the IFT. Neubauer et al. (2020 b) reported a similar influence on IFT behavior for nanofluid that contains the same nanoparticles in nanofluid R1. Another research showed that the silica NPs and surfactants substantially affect IFT reduction (Ma et al., 2008).

Furthermore, nanofluids can improve the materials that lose their efficiency at high salinity. Adding surfactants to nanoparticles is to stabilize the performance of nanofluids in high salinity. Hence, the results show that the effect of salinity does not affect the performance of nanofluids R1, where the difference between real and softened brine of IFT reduction was very low by 0.2 mN/m at concentrations 1 and 2 gpt. Similar results were reported for SiO<sub>2</sub> alkali by (Dahkaee et al., 2019).

However, the result showed that IFT in nanofluid R1 real is lower than and softened, even though real has divalent cations. It can be concluded that the presence of divalent cations ( $\text{Ca}^{2+}$  and  $\text{Mg}^{2+}$ ) in brine plays a vital role and causes a reduction in IFT in the presence of surfactant. The reason could be that the divalent cations have the same electric charge, which increases the surfactant's electric charge to compress the interfacial double layer. Therefore, the repulsion between surfactant molecules increases with the same charge in the micelle, where increase the radius of the micelle particle by more surfactant molecules could enter the micelle, which in result IFT decrease (Hosseini et al., 2015).

Nanofluid S1 and R1 in terms of IFT reduction show that nanofluid R1 has lower IFT than Nanofluid S1. The reason is that nanofluid R1 has  $\text{SiO}_2$  NPs with a surfactant, where NPs can carry the molecular of the surfactant and diffusion towards the oil/ water interface.

**Nanofluid E100** softened showed has low IFT  $\sim 0.233$  mN/m. IFT reduction is attributed to the accumulation of particles at the low TAN oil/softened brine interface.

**Nanofluid A1** contains aluminum oxide ( $\text{Al}_2\text{O}_3$ ) and silicon oxide ( $\text{SiO}_2$ ) nanoparticles with surface-modified. It showed that nanofluid A1 softened has a slightly lower IFT compared to nanofluid S1, R1, and E100. Also, IFT in nanofluid A1 between real and softened are almost the same. This indicates that the effect of salinity with a high and low concentration of divalent cations does not affect the performance of nanofluids. Dahkaee et al. (2019) reported a similar result, the effect of  $\text{NiO}/\text{SiO}_2$  nanofluids on IFT reduction at different salinity. They found that salinity with divalent cations at different concentrations had negligible impacts on interfacial tension. Besides, a combination of  $\text{NiO}/\text{SiO}_2$  nanofluids has a slightly lower IFT compared to when used  $\text{NiO}$  or  $\text{SiO}_2$  alone.

Furthermore, The aluminum oxide ( $\text{Al}_2\text{O}_3$ ) and silicon oxide ( $\text{SiO}_2$ ) NPs have high adsorption and diffusion into the oil/water interface, and hence IFT is reduced. Also, nanofluid A1 has a small size of nanoparticles. The smaller the nanomaterial size has higher catalytic activity, the greater their Brownian motion and higher thermal conductivity in water (Kim et al., 2016). Therefore, smaller particles have higher adsorb at the oil and water interface, resulting in IFT reduction.



Table 5-9 The summary results of IFT at 73 °C and 7000 rpm between low TAN crude oil and nanofluids

	IFT mN/m			
	Mean	SD	min	max
Real Brine - Low TAN oil	10.85	0.56	9.66	12.72
Softened Brine - Low TAN oil	7.14	0.35	6.65	7.98
Nanofluid S1, 10wt%- Low TAN oil	0.429	0.011	0.39	0.47
Nanofluid S1, 15wt%- Low TAN oil	0.476	0.0098	0.44	0.5
Nanofluid S1, 20wt%- Low TAN oil	0.475	0.0097	0.45	0.49
Nanofluid S1, 25wt%- Low TAN oil	0.537	0.051	0.46	0.69
Nanofluid S1, 30wt%- Low TAN oil	0.532	0.0134	0.51	0.56
Nanofluid R1 1gpt Real-Low TAN oil	0.1903	0.0037	0.16	0.2
Nanofluid R1 1gpt Softened-Low TAN oil	0.3458	0.056	0.33	0.41
Nanofluid R1 2gpt Real-Low TAN oil	0.176	0.0023	0.15	0.21
Nanofluid R1 2gpt Softened-Low TAN oil	0.4668	0.042	0.4	0.55
E100 0.1wt% Real-Low TAN oil	6.46	0.65	3.53	7.16
E100 0.1wt% Softened-Low TAN oil	0.233	0.035	0.16	0.37
Nanofluid A1, 10wt% Real-Low TAN oil	0.215	0.01	0.18	0.25
Nanofluid A1, 10wt% Softened-Low TAN oil	0.223	0.0056	0.21	0.25



# Chapter 6

## Conclusion

The conclusions drawn during this study are summarized and presented in a way that addresses the research objective.

The reviewed literature shows that nanoparticles have been considered potential agents to enhance oil recovery. They have unique properties such as small size, high surface area, low costs, and environmentally friendly. The stability of nanoparticle dispersion is one of the key issues that need to be addressed. Nanoparticle SiO<sub>2</sub> is considered the most researched for EOR applications and has massive potential in enhanced oil recovery for sandstone and carbonate reservoirs. Also, there are other metal oxides NPs such as Al<sub>2</sub>O<sub>3</sub>, CuO, and TiO<sub>2</sub>, where the authors examined the potential of NPs. Recently, studies have explored that using nanofluid mixtures lead to improve recovery as they combine the benefits of various NPs.

Nanofluids that do not have any precipitation during fluid preparation with softened brine due to softened brine have less concentration of divalent cation of Ca<sup>+2</sup>. The divalent cations of Ca<sup>+2</sup> and Mg<sup>+2</sup> are the most effective in destabilizing particles, causing aggregation of the nanoparticle and reducing electrostatic repulsions between the particles. Also, high temperatures cause an increased aggregation of nanoparticles. For this reason, nanofluids have precipitation after exposure to high temperatures and salinity. Also, the precipitation of nanofluid A2 in real and softened brine might be due to surface modification, which might be unable to stable nanoparticle at high temperature and salinity in contrast to nanofluid A1 that has not precipitation.

During fluid preparation, the results illustrate that sodium carbonate Na<sub>2</sub>CO<sub>3</sub> has immediate floc formation that was prepared by real brine rich in divalent cations Ca<sup>+2</sup> and Mg<sup>+2</sup>. Hence, sodium carbonate reacted with carbonate, which in result precipitation and aggregation of CaCO<sub>3</sub>. Therefore, it is quite challenging to use an alkaline solution in real brine for other experiments such as phase behavior experiments, IFT, dynamic viscosity, and density

measurements. In contrast, softened brine does not show any precipitation because softened brine contains an ultra-low percentage of  $\text{Ca}^{+2}$ .

Pickering emulsions' stability is influenced by a variety of factors such as the type and concentration of nanoparticles, temperature, the composition of the oleic phase, and the salinity of the brine phase. The divalent cations  $\text{Ca}^{+2}$  and  $\text{Mg}^{+2}$  play a significant role in the stability of Pickering emulsions. Furthermore, A high emulsion volume of most nanofluids was observed directly after mixing samples. Some nanofluids such as R1, E100, and P100 were unable to generate a considerable emulsion volume. The brownish color and turbidity in the aqueous phase might indicate a loss of NSO-compounds or lost aliphatic and aromatic compounds. Even though sodium carbonate  $\text{Na}_2\text{CO}_3$  in softened brine does not have any precipitation due to the low concentration of divalent cation  $\text{Ca}^{+2}$ , sodium carbonate  $\text{Na}_2\text{CO}_3$  could not generate the volume of emulsions that might be due to a low TAN in crude oil. Hence, alkali could not react with oil at the oil/water interface.

The result obtained from Interfacial tension showed that nanofluids were very effective in terms of IFT reduction. The IFT reduction by nanofluids is strongly dependent on its type of nanoparticles, while nanoparticles' concentration and size showed no difference in IFT reduction. Moreover, nanofluid R1 that contains NPs with a surfactant was the most effective on the IFT reduction. It was the lowest value of the IFT, which is approximately 0.17 mN/m compared to other nanofluids. Besides, the IFT between nanofluid A1 that contains  $\text{Al}_2\text{O}_3$  and silica oxide  $\text{SiO}_2$  and crude oil was lower than nanofluids that contain only silica particles with different surface modifications.

## 6.1 Future Work

This work's observations helped to assess the nanofluids that played an essential role in the compatibility test, phase behavior, and IFT test. There are some of the factors that need to be investigated in future work.

- Perform contact angle measurements to determine the initial wettability state.
- Understanding and further implementing workflows for the core flood evaluation and screen EOR chemical blends in carbonate reservoirs with low TAN oil.
- Numerical simulation of the results.
- Assess the use of nanomaterials from an HSE viewpoint.

# Chapter 7

## References

- Aboofazeli, R. (2010). Nanometric-Scaled Emulsions (Nanoemulsions). *Iran J Pharm Res.*, 9.4(1735–0328), 325–326.
- Alnarabiji, M. S., & Husein, M. M. (2020). Application of bare nanoparticle-based nanofluids in enhanced oil recovery. *Fuel*, 267(November 2019), 117262. <https://doi.org/10.1016/j.fuel.2020.117262>
- Al-Attar, H. H., Mahmoud, M. Y., Zekri, A. Y., Almehaideb, R., & Ghannam, M. T. (2013). The impact of LoSal™ on oil recovery from a selected carbonate reservoir in Abu Dhabi - An Experimental Approach. *SPE Middle East Oil and Gas Show and Conference, MEOS, Proceedings*, 2(March), 1404–1417. <https://doi.org/10.2118/164331-ms>
- Arab, D., Kantzas, A., & Bryant, S. L. (2018). Nanoparticle stabilized oil in water emulsions: A critical review. *Journal of Petroleum Science and Engineering*, 163(December 2017), 217–242. <https://doi.org/10.1016/j.petrol.2017.12.091>
- Arditty, S., Schmitt, V., Giermanska-Kahn, J., & Leal-Calderon, F. (2004). Materials based on solid-stabilized emulsions. *Journal of Colloid and Interface Science*, 275(2), 659–664. <https://doi.org/10.1016/j.jcis.2004.03.001>
- Armgate. (2015). SVM 3000 Stabinger Viscometer. <https://www.armgate.lv/en/products/laboratory-equipment/viscometers/kinematic-viscosity-svm-3000-stabinger-viscometer-00209.html>
- Arekhov, V. (2019). Understanding Wettability Changes during Alkali-Polymer through Spontaneous Imbibition Data (Issue May).
- Azadgoleh, J. E., Kharrat, R., Barati, N., & Sobhani, A. (2014). Stability of Silica Nanoparticle Dispersion in Brine Solution : an Experimental Study. *Iranian Journal of Oil & Gas Science and Technology*, 3(4), 26–40.

- Beliveau, D. (2009). Waterflooding viscous oil reservoirs. *SPE Reservoir Evaluation and Engineering*, 12(5), 689–701. <https://doi.org/10.2118/113132-PA>
- Bryan, J., Shamekhi, H., Su, S., & Kantzas, A. (2013). Insights into heavy oil recovery by surfactant, polymer and ASP flooding. *Society of Petroleum Engineers - SPE Heavy Oil Conference Canada 2013*, 1(1993), 631–645. <https://doi.org/10.2118/165440-ms>
- Cheraghian, G., Khalili Nezhad, S. S., Kamari, M., Hemmati, M., Masihi, M., & Bazgir, S. (2014). Adsorption polymer on reservoir rock and role of the nanoparticles, clay and SiO<sub>2</sub>. *International Nano Letters*, 4(3). <https://doi.org/10.1007/s40089-014-0114-7>
- Cheraghian, G., & Hendraningrat, L. (2016). A review on applications of nanotechnology in the enhanced oil recovery part A: effects of nanoparticles on interfacial tension. *International Nano Letters*, 6(2), 129–138. <https://doi.org/10.1007/s40089-015-0173-4>
- Chun Huh, Hugh Daigle, V. P., & Prodanović, and M. (2019). *Practical Nanotechnology for Petroleum Engineers*.
- Chuo, S. C., Ahmad, A., Mohd-Setapar, S. H., & Ripin, A. (2014). Reverse micelle extraction-an alternative for recovering antibiotics. *Der Pharma Chemica*, 6(4), 37–44.
- Dahkaee, K. P., Sadeghi, M. T., Fakhroueian, Z., & Esmailzadeh, P. (2019). Effect of NiO/SiO<sub>2</sub> nanofluids on the ultra interfacial tension reduction between heavy oil and aqueous solution and their use for wettability alteration of carbonate rocks. *Journal of Petroleum Science and Engineering*, 176(January), 11–26. <https://doi.org/10.1016/j.petrol.2019.01.024>
- David Tambe, M. S. (1993). Factors Controlling the Stability of Colloid-Stabilized Emulsions. *Journal of Colloid and Interface Science*, 157(1), 244–253. <https://doi.org/https://doi.org/10.1006/jcis.1993.1182>
- deZabala, E. F., Vislocky, J. M., Rubin, E., & Radke, C. J. (1982). Chemical Theory for Linear Alkaline Flooding. *Society of Petroleum Engineers Journal*, 22(2), 245–258. <https://doi.org/10.2118/8997-pa>
- Divandari, H., Hemmati-Sarapardeh, A., Schaffie, M., & Ranjbar, M. (2020). Integrating functionalized magnetite nanoparticles with low salinity water and surfactant solution: Interfacial tension study. *Fuel*, 281(July). <https://doi.org/10.1016/j.fuel.2020.118641>
- Esfandyari Bayat, A., Junin, R., Samsuri, A., Piroozian, A., & Hokmabadi, M. (2014). Impact of metal oxide nanoparticles on enhanced oil recovery from limestone media at several temperatures. *Energy and Fuels*, 28(10), 6255–6266. <https://doi.org/10.1021/ef5013616>

- Gbadamosi, A. O., Junin, R., Manan, M. A., Agi, A., & Yusuff, A. S. (2019). An overview of chemical enhanced oil recovery: recent advances and prospects. In *International Nano Letters* (Vol. 9, Issue 3). Springer Berlin Heidelberg. <https://doi.org/10.1007/s40089-019-0272-8>
- Esmaeilzadeh, P., Hosseinpour, N., Bahramian, A., Fakhroueian, Z., & Arya, S. (2014). Effect of ZrO<sub>2</sub> nanoparticles on the interfacial behavior of surfactant solutions at air-water and n-heptane-water interfaces. *Fluid Phase Equilibria*, 361, 289–295. <https://doi.org/10.1016/j.fluid.2013.11.014>
- Goodarzi, F., & Zendejboudi, S. (2019). A Comprehensive Review on Emulsions and Emulsion Stability in Chemical and Energy Industries. *Canadian Journal of Chemical Engineering*, 97(1), 281–309. <https://doi.org/10.1002/cjce.23336>
- Grutters, M., van Dijk, M., Dubey, S., Adamski, R., Gelin, F., & Cornelisse, P. (2007). Asphaltene induced w/o emulsion: False or true? *Journal of Dispersion Science and Technology*, 28(3), 357–360. <https://doi.org/10.1080/01932690601107658>
- Guo, H., Dou, M., Hanqing, W., Wang, F., Yuanyuan, G., Yu, Z., Yansheng, W., & Li, Y. (2017). Proper Use of Capillary Number in Chemical Flooding. *Journal of Chemistry*, 2017. <https://doi.org/10.1155/2017/4307368>
- Ha, S. W., Camalier, C. E., Beck, G. R., & Lee, J. K. (2009). New method to prepare very stable and biocompatible fluorescent silica nanoparticles. *Chemical Communications*, 20, 2881–2883. <https://doi.org/10.1039/b902195g>
- Healy, R. N., Reed, R. L., & Carpenter, C. W. (1975). Laboratory Study of Microemulsion Flooding. *Soc Pet Eng AIME J*, 15(1), 87–103.
- Hassan, M. E., Nielsen, R. F., & Calhoun, J. C. (1953). Effect of Pressure and Temperature on Oil-Water Interfacial Tensions for a Series of Hydrocarbons. *Journal of Petroleum Technology*, 5(12), 299–306. <https://doi.org/10.2118/298-g>
- Hendraningrat, L., & Torsæter, O. (2014). Unlocking the potential of metal oxides nanoparticles to enhance the oil recovery. *Proceedings of the Annual Offshore Technology Conference*, 1(2013), 211–222. <https://doi.org/10.4043/24696-ms>
- Jalil, R. R., & Hussein, H. (2019). Influence of Nano Fluid on Interfacial Tension oil/water and Wettability Alteration of limestone. *IOP Conference Series: Materials Science and Engineering*, 518(6). <https://doi.org/10.1088/1757-899X/518/6/062004>
- Hosseini, S. N., Shuker, M. T., Hosseini, Z., Joao Tomocene, T., Shabib-asl, A., & Sabet, M. (2015). The role of salinity and brine ions in interfacial tension reduction while using surfactant for enhanced oil recovery. *Research Journal of Applied Sciences, Engineering and Technology*, 9(9), 722–726. <https://doi.org/10.19026/rjaset.9.2617>

- Jeng, J. F., & Miller, C. A. (1987). Theory of microemulsions with spherical drops I. Phase diagrams and interfacial tensions in gravity-free systems. *Colloids and Surfaces*, 28(C), 247–269. [https://doi.org/10.1016/0166-6622\(87\)80188-9](https://doi.org/10.1016/0166-6622(87)80188-9)
- Joonaki, E., & Ghanaatian, S. (2014). The application of nanofluids for enhanced oil recovery: Effects on interfacial tension and coreflooding process. *Petroleum Science and Technology*, 32(21), 2599–2607. <https://doi.org/10.1080/10916466.2013.855228>
- Kamal, M. S., Adewunmi, A. A., Sultan, A. S., Al-Hamad, M. F., & Mehmood, U. (2017). Recent advances in nanoparticles enhanced oil recovery: Rheology, interfacial tension, oil recovery, and wettability alteration. *Journal of Nanomaterials*, 2017(October). <https://doi.org/10.1155/2017/2473175>
- Kim, I., Worthen, A. J., Johnston, K. P., DiCarlo, D. A., & Huh, C. (2016). Size-dependent properties of silica nanoparticles for Pickering stabilization of emulsions and foams. *Journal of Nanoparticle Research*, 18(4), 1–12. <https://doi.org/10.1007/s11051-016-3395-0>
- Krüß scientific. (2018). Spinning Drop Tensiometer SDT - KRÜSS GmbH.
- Kumar, S., Yen, T. F., Chilingarian, G. V., & Donaldson, E. C. (1989). Alkaline Flooding. *Developments in Petroleum Science*, 17(PB), 219–254. [https://doi.org/10.1016/S0376-7361\(08\)70461-8](https://doi.org/10.1016/S0376-7361(08)70461-8)
- Leitenmüller, V., & Rupprecht, B. J. (2019). Journal of Petroleum Science and Engineering A multidisciplinary approach for chemical EOR screening : Understanding alkali-oil interaction by the use of petroleum geochemistry. *Journal of Petroleum Science and Engineering*, 180(June), 967–981. <https://doi.org/10.1016/j.petrol.2019.06.018>
- Li, S., Ng, Y. H., Lau, H. C., Torsæter, O., & Stubbs, L. P. (2020). Experimental investigation of stability of silica nanoparticles at reservoir conditions for enhanced oil-recovery applications. *Nanomaterials*, 10(8), 1–15. <https://doi.org/10.3390/nano10081522>
- Ma, H., Luo, M., & Dai, L. L. (2008). Influences of surfactant and nanoparticle assembly on effective interfacial tensions. *Physical Chemistry Chemical Physics*, 10(16), 2207–2213. <https://doi.org/10.1039/b718427c>
- Mahmoudi, S., Jafari, A., & Javadian, S. (2019). Temperature effect on performance of nanoparticle/surfactant flooding in enhanced heavy oil recovery. *Petroleum Science*, 16(6), 1387–1402. <https://doi.org/10.1007/s12182-019-00364-6>
- McElfresh, P., Holcomb, D., & Ector, D. (2012). Application of nanofluid technology to improve recovery in oil and gas wells. *Society of Petroleum Engineers - SPE International Oilfield Nanotechnology Conference 2012*, 2003, 46–51. <https://doi.org/10.2118/154827-ms>



- Mcmullen, R. L., & Ingredients, A. S. (2014). SECTION II : Formulation , Processing and Production Techniques. January, 129–154.
- Metin, C. O., Lake, L. W., Miranda, C. R., & Nguyen, Q. P. (2011). Stability of aqueous silica nanoparticle dispersions. *Journal of Nanoparticle Research*, 13(2), 839–850. <https://doi.org/10.1007/s11051-010-0085-1>
- Mohamed, S. G., Souliman, M. M., Hamid, M., & Tantawy, M. A. (2018). Investigating The Application of Nano Particles for Enhanced Oil Recovery. 9(8), 1585–1603.
- Munir, R., Syed, H. K., Asghar, S., Khan, I. U., Rasul, A., Irfan, M., & Sadique, A. (2017). Microemulsion: promising and novel system for drug delivery. *J Toxicol Pharmaceut Sci*, 1(2), 128–134.
- Neubauer, E., Hincapie, R. E., Borovina, A., Biernat, M., Clemens, T., & Ahmad, Y. K. (2020). Influence of Nanofluids on Wettability Changes and Interfacial Tension Reduction. 1–14. <https://doi.org/10.2118/200643-ms>
- Neubauer, E., Hincapie, R. E., Clemens, T., Omv, E., Cornelius, M., & Resource, E. (2020). SPE-200411-MS Selection of Nanomaterials as Emulsion Stabilizers in Alkali-Polymer EOR of High-TAN Number Oil.
- Ogolo, N. A., Olafuyi, O. A., Onyekonwu, M. O., Technology, P., & Fund, D. (2012). Spe-160847-MS. *SPE Journal*, 1–9. <https://doi.org/10.2118/160847-MS>
- Olayiwola, S. O., & Dejam, M. (2019). A comprehensive review on interaction of nanoparticles with low salinity water and surfactant for enhanced oil recovery in sandstone and carbonate reservoirs. *Fuel*, 241(October 2018), 1045–1057. <https://doi.org/10.1016/j.fuel.2018.12.122>
- Pal, S., Mushtaq, M., Banat, F., & Al Sumaiti, A. M. (2018). Review of surfactant-assisted chemical enhanced oil recovery for carbonate reservoirs: challenges and future perspectives. *Petroleum Science*, 15(1), 77–102. <https://doi.org/10.1007/s12182-017-0198-6>
- Park, L. K. E., Liu, J., Yiacoumi, S., Borole, A. P., & Tsouris, C. (2017). Contribution of acidic components to the total acid number (TAN) of bio-oil. *Fuel*, 200, 171–181. <https://doi.org/10.1016/j.fuel.2017.03.022>
- Rostami, P., Mehraban, M. F., Sharifi, M., Dejam, M., & Ayatollahi, S. (2019). Effect of water salinity on oil/brine interfacial behaviour during low salinity waterflooding: A mechanistic study. *Petroleum*, 5(4), 367–374. <https://doi.org/10.1016/j.petlm.2019.03.005>
- Saien, J., & Bahrami, M. (2016). Understanding the effect of different size silica nanoparticles and SDS surfactant mixtures on interfacial tension of n-hexane–water. *Journal of Molecular Liquids*, 224, 158–164. <https://doi.org/10.1016/j.molliq.2016.09.112>

- Samanta, A., Ojha, K., & Mandal, A. (2011). Interactions between acidic crude oil and alkali and their effects on enhanced oil recovery. *Energy and Fuels*, 25(4), 1642–1649. <https://doi.org/10.1021/ef101729f>
- Samuel Boyle. (2016). Nissan Chemical America Corporation. <https://www.nanoactiv.com/products/nanoactiv-eft>
- SHARMA, M. K., & SHAH, D. O. (1985). Introduction to Macro- and Microemulsions. 1–18. <https://doi.org/10.1021/bk-1985-0272.ch001>
- Sharma, M. M., Jang, L. K., & Yen, T. F. (1984). Transient Interfacial Tension Behavior of Crude Oil Caustic Interfaces. *Society of Petroleum Engineers of AIME*, (Paper) SPE, 1(May), 377–389.
- Sheng. (2014). Membrane reactors – Part I. *Technology*, 17, 471–489. <https://doi.org/10.1002/apj>
- Sheng, J. J. (2015). Investigation of alkaline–crude oil reaction. *Petroleum*, 1(1), 31–39. <https://doi.org/10.1016/j.petlm.2015.04.004>
- Sheng, J. J. (2013). Alkaline-Polymer Flooding. In *Enhanced Oil Recovery Field Case Studies (First Edit)*. Elsevier Inc. <https://doi.org/10.1016/B978-0-12-386545-8.00007-5>
- Singh, S., & Ahmed, R. (2010). Vital role of nanopolymers in drilling and stimulations fluid applications. *Proceedings - SPE Annual Technical Conference and Exhibition*, 1(September), 71–77. <https://doi.org/10.2118/130413-ms>
- Spanos, N., & Koutsoukos, P. G. (1998). Kinetics of precipitation of calcium carbonate in alkaline pH at constant supersaturation. Spontaneous and seeded growth. *Journal of Physical Chemistry B*, 102(34), 6679–6684. <https://doi.org/10.1021/jp981171h>
- Sofla, S. J. D., James, L. A., & Zhang, Y. (2019). Understanding the behavior of H<sup>+</sup>-protected silica nanoparticles at the oil-water interface for enhanced oil recovery (EOR) applications. *Journal of Molecular Liquids*, 274, 98–114. <https://doi.org/10.1016/j.molliq.2018.09.049>
- Sun, X., Zhang, Y., Chen, G., & Gai, Z. (2017). Application of nanoparticles in enhanced oil recovery: A critical review of recent progress. *Energies*, 10(3). <https://doi.org/10.3390/en10030345>
- Thomas, N. C., Ghosh, B., Alameri, W. S., & Kilybay, A. (2016). Alkali and Hybrid-Alkali Flooding as a Tertiary Oil Recovery Mode: Prospects and Challenges. *International Journal of Petroleum and Petrochemical Engineering*, 2(2), 22–31. <https://doi.org/10.20431/2454-7980.0202005>

- Tarek, M. (2015). Investigating nano-fluid mixture effects to enhance oil recovery. *Proceedings - SPE Annual Technical Conference and Exhibition, 2015-Janua*, 6803–6813. <https://doi.org/10.2118/178739-stu>
- Viades-Trejo, J., & Gracia-Fadrique, J. (2007). Spinning drop method. From Young-Laplace to Vonnegut. *Colloids and Surfaces A: Physicochemical and Engineering Aspects*, 302(1–3), 549–552. <https://doi.org/10.1016/j.colsurfa.2007.03.033>
- Vonnegut, B. (1942). Rotating bubble method for the determination of surface and interfacial tensions. *Review of Scientific Instruments*, 13(1), 6–9. <https://doi.org/10.1063/1.1769937>
- Wang, X., & Alvarado, V. (2008). Effect of salinity and pH on pickering emulsion stability. *Proceedings - SPE Annual Technical Conference and Exhibition*, 4(September), 2676–2692. <https://doi.org/10.2118/115941-ms>
- Wang, Y., Xu, H., Yu, W., Bai, B., Song, X., & Zhang, J. (2011). Surfactant induced reservoir wettability alteration: Recent theoretical and experimental advances in enhanced oil recovery. *Petroleum Science*, 8(4), 463–476. <https://doi.org/10.1007/s12182-011-0164-7>
- Wang, Z., Babadagli, T., & Maeda, N. (2020). Preliminary Screening and Formulation of New Generation Nanoparticles for Stable Pickering Emulsion in Cold and Hot Heavy-Oil Recovery. *SPE Reservoir Evaluation & Engineering*, November 2019, 9–11. <https://doi.org/10.2118/200190-pa>
- Wasan, D., Nikolov, A., & Kondiparty, K. (2011). The wetting and spreading of nanofluids on solids: Role of the structural disjoining pressure. *Current Opinion in Colloid and Interface Science*, 16(4), 344–349. <https://doi.org/10.1016/j.cocis.2011.02.001>
- Wei, B., Li, Q., Jin, F., Li, H., & Wang, C. (2016). The Potential of a Novel Nanofluid in Enhancing Oil Recovery. *Energy and Fuels*, 30(4), 2882–2891. <https://doi.org/10.1021/acs.energyfuels.6b00244>
- Yang, Y., Fang, Z., Chen, X., Zhang, W., Xie, Y., Chen, Y., Liu, Z., & Yuan, W. (2017). An overview of pickering emulsions: Solid-particle materials, classification, morphology, and applications. *Frontiers in Pharmacology*, 8(MAY), 1–20. <https://doi.org/10.3389/fphar.2017.00287>
- Yu, W., & Xie, H. (2012). A review on nanofluids: Preparation, stability mechanisms, and applications. *Journal of Nanomaterials*, 2012. <https://doi.org/10.1155/2012/435873>
- Zargartalebi, M., Kharrat, R., & Barati, N. (2015). Enhancement of surfactant flooding performance by the use of silica nanoparticles. *Fuel*, 143, 21–27. <https://doi.org/10.1016/j.fuel.2014.11.040>

- Zhang, H., Nikolov, A., & Wasan, D. (2014). Enhanced oil recovery (EOR) using nanoparticle dispersions: Underlying mechanism and imbibition experiments. *Energy and Fuels*, 28(5), 3002–3009. <https://doi.org/10.1021/ef500272r>
- Zhao, M., Lv, W., Li, Y., Dai, C., Zhou, H., Song, X., & Wu, Y. (2018). A study on preparation and stabilizing mechanism of hydrophobic silica nanofluids. *Materials*, 11(8). <https://doi.org/10.3390/ma11081385>

# Appendix A

## Lab Experiments Results

### A.1 Fluids Properties

#### 1. Sodium Carbonate $\text{Na}_2\text{CO}_3$ considered as the alkali solution

Table 7-1  $\text{Na}_2\text{CO}_3$  properties

	Dynamic viscosity, (mPs.s)				Density, (g/cm <sup>3</sup> )				
	25C°		73C°		25C°		73C°		
	Mean	SD	Mean	SD	Mean	SD	Mean	SD	
Sodium carbonate softened, 1000 ppm	Na <sub>2</sub> CO <sub>3</sub>	1.1354	0.1044	0.5341	0.0898	1.0437	0.0006	1.0232	0.0013
Sodium carbonate softened, 2000 ppm	Na <sub>2</sub> CO <sub>3</sub>	1.0839	0.0302	0.5050	0.0167	1.0464	0.0012	1.0246	0.0022
Sodium carbonate softened, 3000 ppm	Na <sub>2</sub> CO <sub>3</sub>	1.0621	0.0020	0.6342	0.2358	1.0466	0.0005	1.0249	0.0014
Sodium carbonate softened, 4000 ppm	Na <sub>2</sub> CO <sub>3</sub>	1.0611	0.0135	0.4934	0.0120	1.0475	0.0012	1.0260	0.0018
Sodium carbonate softened, 5000 ppm	Na <sub>2</sub> CO <sub>3</sub>	1.0717	0.0024	0.5088	0.0124	1.0475	0.0006	1.0259	0.0014
Sodium carbonate softened, 6000 ppm	Na <sub>2</sub> CO <sub>3</sub>	1.0728	0.0015	0.5036	0.0031	1.0486	0.0008	1.0272	0.0012

Sodium carbonate Na <sub>2</sub> CO <sub>3</sub> softened, 7000 ppm	1.0553	0.0206	0.5151	0.0154	1.0496	0.0008	1.0281	0.0012
Sodium carbonate Na <sub>2</sub> CO <sub>3</sub> softened, 8000 ppm	1.0759	0.0152	0.5007	0.0137	1.0512	0.0015	1.0300	0.0034
Sodium carbonate Na <sub>2</sub> CO <sub>3</sub> softened, 9000 ppm	1.0867	0.0030	0.5128	0.0015	1.0519	0.0008	1.0300	0.0013
Sodium carbonate Na <sub>2</sub> CO <sub>3</sub> softened, 10,000 ppm	1.0950	0.0087	0.5109	0.0081	1.0537	0.0017	1.0316	0.0025

**2. Nanofluids**

Table 7-2 Nano clear A1 & A2

	Dyainmic viscosity, (mPs.s)				Density, (g/cm3)			
	25C°		73C°		25C°		73C°	
	Mean	SD	Mean	SD	Mean	SD	Mean	SD
Nanofluid A1 Real, 10 wt%	1.2263	0.0857	0.5102	0.0022	1.0418	0.0002	1.0199	0.0004
Nanofluid A1 Softened, 10 wt%	1.0761	0.0037	0.4952	0.0008	1.0337	0.0002	1.0121	0.0004
Nanofluid A1 Real, 20 wt%	1.2633	0.1201	0.5583	0.0995	1.0466	0.0003	1.0243	0.0004
Nanofluid A1 Softened, 20 wt%	1.1954	0.1470	0.5624	0.1262	1.0377	0.0003	1.0156	0.0007
Nanofluid A2 Real, 10 wt%	1.6584	0.0701	0.7375	0.1367	1.0510	0.0005	1.0286	0.0013
Nanofluid A2 Softened, 10 wt%	1.1609	0.0580	0.5494	0.0095	1.0434	0.0006	1.0214	0.0014
Nanofluid A2 Real, 20 wt%	2.1710	0.2960	1.0561	0.3468	1.0484	0.0019	1.0258	0.0013
Nanofluid A2 Softened, 20 wt%	1.2978	0.1618	0.5727	0.0523	1.0429	0.0004	1.0217	0.0009

Table 7-3: Nanofluids E100 & P100

	Dyainmic viscosity, (mPs.s)				Density, (g/cm3)			
	25C°		73C°		25C°		73C°	
	Mean	SD	Mean	SD	Mean	SD	Mean	SD
E100 Real, 0,1 wt%	1.8624	0.9545	1.4345	1.6135	1.0511	0.0002	1.0290	0.0008
E100 Softened,0,1 wt%	1.0479	0.0074	0.4956	0.0167	1.0402	0.0006	1.0198	0.0006
P100 Real, 0,1 wt%	1.4283	0.1410	0.5858	0.1353	1.0515	0.0002	1.0296	0.0008

P100 Softened,0,1 wt%	1.2592	0.1338	0.5729	0.1540	1.0416	0.0003	1.0202	0.0007
-----------------------	--------	--------	--------	--------	--------	--------	--------	--------

Table 7-4: Nanofluid R1 at 1 & 2 gpt for real and softened

	Dyainmic viscosity, (mPs.s)				Density, (g/cm3)			
	25C°		73C°		25C°		73C°	
	Mean	SD	Mean	SD	Mean	SD	Mean	SD
Nanofluid R1 real, 1 gpt	1.2164	0.0864	0.5046	0.0143	1.0506	0.0001	1.0289	0.0006
Nanofluid R1 real, 2 gpt	1.0977	0.0121	0.5090	0.0072	1.0502	0.0002	1.0287	0.0004
Nanofluid R1 softened, 1 gpt	1.0815	0.0320	0.4982	0.0165	1.0406	0.0004	1.0191	0.0007
Nanofluid R1 softened, 2 gpt	1.0347	0.0046	0.4809	0.0074	1.0406	0.0006	1.0195	0.0012

Table 7-5: Nanofluid (S1) at different concentrations for real & softened

	Dyainmic viscosity, (mPs.s)				Density, (g/cm3)			
	25C°		73C°		25C°		73C°	
	Mean	SD	Mean	SD	Mean	SD	Mean	SD
Nanofluid S1 softened, 10 wt%	1.1205	0.0057	0.5211	0.0055	1.0516	0.0006	1.0305	0.0003
Nanofluid S1 softened, 15 wt%	1.2663	0.0543	0.5431	0.0054	1.0578	0.0007	1.0358	0.0016
Nanofluid S1 softened, 20 wt%	1.2631	0.0303	0.5767	0.0233	1.0633	0.0008	1.0412	0.0013
Nanofluid S1 softened, 25 wt%	1.3513	0.0343	0.5976	0.0210	1.0692	0.0008	1.0470	0.0013
Nanofluid S1 softened, 30 wt%	1.5035	0.0408	0.6216	0.0209	1.0752	0.0008	1.0530	0.0015
Nanofluid S1 Real, 10 wt%	1.1790	0.0080	0.5648	0.0151	1.0597	0.0006	1.0392	0.0005

Nanofluid S1 Real, 15 wt%	1.2471	0.0085	0.6016	0.0198	1.0665	0.0007	1.0453	0.0014
Nanofluid S1Real, 20 wt%	1.3177	0.0097	0.6205	0.0122	1.0718	0.0008	1.0497	0.0011
Nanofluid S1 Real, 25 wt%	1.3892	0.0104	0.6292	0.0057	1.0770	0.0007	1.0547	0.0014
Nanofluid S1 Real, 30 wt%	1.4732	0.0154	0.7255	0.0984	1.0828	0.0011	1.0606	0.0021



